eprints@whiterose.ac.uk
https://eprints.whiterose.ac.uk/

An Excel tool for deriving key photosynthetic parameters from combined gas exchange and chlorophyll fluorescence: theory and practice

Chandra Bellasio[1*], David J Beerling[1] and Howard Griffiths[2]

1 Department of Animal and Plant Sciences, University of Sheffield, Sheffield, S10 2TN, UK

2 Department of Plant Sciences, university of Cambridge, Cambridge, CB2 3EA, UK

*Correspondence: c.bellasio@sheffield.ac.uk

Abstract:

Combined photosynthetic gas exchange and modulated fluorometers are widely used to evaluate physiological characteristics associated with phenotypic and genotypic variation, whether in response to genetic manipulation or resource limitation in natural vegetation or crops. After describing relatively simple experimental procedures, we present the theoretical background to the derivation of photosynthetic parameters, and provide a freely available Excel Fitting Tool (EFT) that will be of use to specialists and non-specialists alike. We use data acquired in concurrent variable fluorescence - gas exchange experiments, where A/C_i and light-response curves have been measured under ambient and low oxygen. From these data, the EFT derives light-respiration, initial PSII photochemical yield, initial quantum yield for CO_2 fixation, fraction of incident light harvested by PSII, initial quantum yield for electron transport, electron transport rate, rate of photorespiration, stomatal limitation, Rubisco rate of carboxylation and oxygenation, Rubisco specificity factor, mesophyll conductance to CO_2 diffusion, light and CO_2 compensation point, Rubisco apparent Michaelis-Menten constant, and Rubisco CO_2-saturated carboxylation rate. As an example, a complete analysis of gas exchange data on tobacco plants is provided. We also discuss potential measurement problems and pitfalls, and suggest how such empirical data could subsequently be used to parameterise predictive photosynthetic models.

Keywords

Modelling, quantum yield, respiration, compensation point, αβ, electron transport rate, photorespiration, oxygenation, carboxylation, rate, Rubisco, specificity, mesophyll conductance, V_{CMAX}.

Introduction

Leaf photosynthetic gas exchange is generally measured with infra-red gas analysers (IRGA). CO_2 uptake (referred to as net assimilation, A; symbols and acronyms are listed in Table 1) and water vapour transpiration are measured directly. A first data treatment step, embedded in the IRGA software, uses classical calculations (Farquhar *et al.*, 1980, von Caemmerer & Farquhar, 1981) to derive stomatal conductance to H_2O, and then CO_2 (g_S), together with the CO_2 concentration in the substomatal cavity (C_i). In this way, A, g_S and C_i are standard outputs of IRGA measurements, in addition to incident light intensity (*PPFD*) (Evans, 2013, Long & Bernacchi, 2003, Long *et al.*, 1996). All IRGA manufacturers optionally mount a pulse amplitude modulated leaf chamber fluorometer on the IRGA leaf cuvette. These devices add high frequency pulses of 'modulated light' to the background illumination and deconvolute the reflected fluorescence signal, as the dimensionless quantity 'F' representing leaf-level fluorescence yield [see recent comments and refinements: (Harbinson, 2013, Loriaux *et al.*, 2013, Schansker *et al.*, 2014, Stirbet & Govindjee, 2011)]. The photochemical yield of PSII (*Y(II)*) can be measured under continuous *PPFD* (Genty *et al.*, 1989) by comparing the steady state F (F_S) to a maximum (F_M') obtained by artificially 'quenching' *Y(II)* using an instantaneous 'saturating pulse' (8 – 20 mmol photon m^{-1} s^{-1} *PPFD*) which completely reduces Q_A (Baker, 2008, Maxwell & Johnson, 2000, Murchie & Lawson, 2013, Papageorgiou, 2004). Gas exchange can provide additional information if measured in a low O_2 (1.5-2%) background instead of air. Low O_2 suppresses Rubisco oxygenase activity (Eckardt, 2005), thus allowing the rate of Rubisco carboxylation (V_C) to be derived from A and R_{LIGHT} (the rate of 'day' respiration). These techniques can be augmented by real-time isotopic discrimination measurements (Bellasio & Griffiths, 2014b, Cernusak *et al.*, 2013, Gu & Sun, 2014, Tazoe *et al.*, 2011, von Caemmerer *et al.*, 2014), but are not considered further in this paper.

IRGA outputs can be analysed 'descriptively' using photosynthetic models. These describe an output variable (e.g. assimilation A_{MOD}) using 1) measurable input variables (e.g. C_i); 2) a mathematical expression; and 3) parameters representing physiological traits (for instance Rubisco CO_2-saturated rate of carboxylation V_{CMAX}). Parameters may be constant or differ between different groups of plants, depending on the rationale of the experiment. To find the parameter values which 'describe' the response of a given plant, models are 'fitted', i.e. the sum of squared residual (SSE) between the model output and a consistent set of measured data is minimised by iteratively trying different parameter values. These iterations are generally aided by specific software (e.g. we used the Excel package 'Solver'). The fitted parameters provide useful proxies which summarise contrasting photosynthetic responses, and can be statistically treated to highlight differences between plants or treatments. The work of experimental physiologists may be completed at this stage, although models and parameters can be used in a third phase, which we call 'predictive'. Here, photosynthetic characteristics are calculated for conditions which will differ, in space, time or

for environmental factors, to those of the original gas exchange experiment(s). Predictive modelling is important when photosynthesis cannot be measured directly, for instance at the field scale (Bernacchi *et al.*, 2013, Boote *et al.*, 2013, Keurentjes *et al.*, 2013, Yin & Struik, 2010), or at the global scale (Melton *et al.*, 2013, Woodward & Lomas, 2004).

There are a variety of descriptive modelling approaches, and recent research has refined classical models to account for mesophyll diffusion resistances and variable enzyme kinetics (Ethier & Livingston, 2004, Gu *et al.*, 2010, Tholen *et al.*, 2012b). There is a need for these new approaches to be incorporated in predictive models in order to refine estimates of global net productivity (Sun *et al.*, 2014b). However, updating existing data analysis tools with new sub-routines can be difficult because they may not be freely downloadable, use proprietary software, and coding skills are often required to implement modifications (Gu *et al.*, 2010, Laisk *et al.*, 2002, Yin *et al.*, 2009). Furthermore, different modelling logics need to work together, and parameters derived under different experimental conditions may need to be recruited from unrelated studies. The goals of this work were to 1) develop an updated and accessible comprehensive data treatment tool for descriptive modelling; 2) describe the general logic and theory of data analysis including classical and modern approaches; and 3) succinctly demonstrate the current best practices of data analysis and fluorescence-gas exchange measurements.

We implemented an Excel based fitting tool (EFT) that is freely available to download from Supporting Materials. The use of macros is avoided so that all calculations appear in spreadsheet cells, allowing greater transparency and straight forward modification. The EFT derives a suite of advanced photosynthetic parameters using standard gas exchange-fluorescence datasets, and therefore represents a significant advancement for many molecular biologists and ecologists. In addition, the EFT accommodates a wide range of methodological variations for more advanced applications. We first review the theory of gas exchange data analysis then describe how the EFT outputs allow detailed comparisons of photosynthetic characteristics to be made – whether for natural vegetation or plants with engineered photosynthetic traits. A worked analysis of gas exchange data measured on tobacco plants is discussed in the second part of the paper and we detail the gas exchange experiment settings and potential pitfalls in Supporting Information. Finally, we provide a link to a demonstration video tutorial. Although predictive modelling goes beyond the scope of this work, we will mention how the EFT outputs can be used by current or next-generation models.

Measurements and rationale for different O_2 levels

To derive a complete set of physiological parameters with this EFT, four response curves (A/C_i and light-response curves each measured under both ambient and low O_2) are measured consecutively on the same portion of the leaf. Detailed settings and potential issues of gas exchange measurements are provided for guidance in Supporting Information Notes 1 and 2. The rationale for repeating gas

exchange measurements under low O_2 is to suppress photorespiration. In these conditions V_C can be resolved from gross assimilation GA ($GA=A+R_{LIGHT}$) as $V_C=GA$. Since the main sink for reducing power is CO_2 assimilation, the rate of electron transport (J) can then be stoichiometrically derived as $J=4V_C$. Different definitions for J coexist in the literature on photosynthetic modelling, which has led to some ambiguity. Here we define J as the rate of electron transport delivered to $NADP^+$ and used by the photosynthetic RPP and the PCO cycles. The factor 4 results from knowing that reducing each fixed CO_2 requires 2 NADPH, each carrying 2e⁻. With J, a calibration factor between J and $Y(II)$ can be established (Valentini *et al.*, 1995, Yin *et al.*, 2009). That calibration factor allows J to be predicted under photorespiratory conditions, using values of $Y(II)$ measured under ambient O_2.

Development of Theory embedded within the Excel-based Fitting Tool (EFT)

Description of the procedure for deriving parameters

We modified the overall logical path proposed by Yin *et al.* (2009), from concurrent multi-curve fitting to a cascade 'step-by-step' fitting protocol. This was then integrated with recent developments and alternatives proposed by other investigators. Cascade 'step-by-step' means that data analysis is divided into 13 discrete steps (EFT sheets are numbered 1 – 13 accordingly) and each step extracts a new piece of information using parameters previously derived. Light-curves, fluorescence and low O_2 increase the available information eight-fold compared to an ordinary A/C_i curve, provide better model constraints, and reduce the risk of deriving many parameters from a limited number of datapoints (overparameterisation). Discrete steps allow greater control over the output and flexibility in choosing which parameters to derive. The steps are summarised as follows:

1 Data are entered into the EFT and limitations are selected manually.

2 Respiration in the light (R_{LIGHT}) is derived using the initial light-limited portion of the fluorescence-light-curves (Yin *et al.*, 2011a).

3 The initial yield of photosystem II ($Y(II)_{LL}$) is extrapolated under zero $PPFD$ by linear regression of $Y(II)$ in the initial light-limited portion of the fluorescence-light-curves (Yin *et al.*, 2009).

4 Gross assimilation (GA), the net biochemical CO_2 uptake, a key quantity of photosynthetic modelling, is calculated by summing R_{LIGHT} plus A and the $PPFD$ dependence of GA is described empirically by a non-rectangular hyperbola. The maximum quantum yield for CO_2 fixation ($Y(CO_2)_{LL}$) and the light-saturated GA (GA_{SAT}) are estimated by curve-fitting. The $PPFD–A$ compensation point (LCP) is calculated from the fitted curve.

5 An empirical non-rectangular hyperbola is fitted to the A/C_i curves under ambient and low O_2 to estimate the maximal carboxylating efficiency (CE), the $C_i–A$ compensation point (Γ, i.e. the C_i at which A is zero) and $C_i–GA$ compensation point (C_i*, i.e. the C_i at which GA is zero) and CO_2-

4

saturated A (A_{SAT}). The fitted curve is used to assess stomatal limitation to photosynthesis (L_S). The rate of triose phosphate utilisation is calculated (variants available).

6 The fraction of *PPFD* harvested by PSII is derived using two different approaches: the approach of Yin (Yin & Struik, 2009a, Yin *et al.*, 2004) (which fits a quantity called *s*) and the approach of Valentini (Valentini *et al.*, 1995) (which fits a quantity called αβ).

7 With $Y(II)_{LL}$ and either *s* or αβ, the initial quantum yield for electron transport ($Y(J)_{LL}$, conversion efficiency of *PPFD* into *J*) is calculated (Yin *et al.*, 2009).

8 *J* is calculated using *PPFD*, *Y(II)*, and *s* or αβ derived in Step 7 or with a point-to-point approach directly from *GA*.

9 The light-dependence of *J* under ambient O_2 is described by an empirical non-rectangular hyperbola (Yin *et al.*, 2009): $Y(J)_{LL}$ derived in Step 7 defines the initial slope while the curvature, θ, and the light-saturated J_{SAT} are estimated by curve-fitting.

10 With *J* and *A*, all quantities associated with Rubisco activity *in vivo* (rate of carboxylation, oxygenation and photorespiration rate) are calculated for each datapoint (Bellasio *et al.*, 2014) assuming that reducing power is limiting photosynthesis (von Caemmerer, 2000).

11 The *in vivo* Rubisco specificity factor ($S_{C/O}$) is estimated by comparing the previously derived *CE* under ambient and low O_2 (Yin *et al.*, 2009).

12 With $S_{C/O}$, *J* and R_{LIGHT} previously derived, assimilation is modelled (A_{MOD}), and mesophyll conductance to CO_2 diffusion (g_M) is estimated by fitting A_{MOD} to *A* in the light-limited part of A/C_i and light-curves (calculation variants are available).

13 With Γ, g_M, and R_{LIGHT}, the C_C based Rubisco kinetic parameters V_{CMAX} (CO_2-saturated carboxylation rate) and $K_C(1+O/K_O)$ (apparent Michaelis-Menten constant) are estimated by fitting the 'full Farquhar model' as developed by (Ethier & Livingston, 2004) to the Rubisco-limited part of the A/C_i curve. By using information derived in previous steps, this procedure, avoids uncertainties associated with the overparameterization of the Farquhar model (Gu *et al.*, 2010).

Steps 1 – 10 are applicable to any photosynthetic pathway of assimilation such as C_3, C_4, intermediate, C_2, and CAM metabolism (see Intermediate and Engineered assimilatory pathways, below). This is possible because equations relate to NADPH-limited photosynthesis (von Caemmerer, 2000) which are independent of the photosynthetic pathway, and because the mathematical formulation of empirical models is purely based on the external behaviour of the system (Thakur, 1991). Steps 11 – 13 are based on mechanistic models, which are underpinned by the functional mechanisms of the individual biochemical processes and thus will produce meaningful results only for the C_3 assimilatory physiology. We will now describe the practical use of the EFT, together with theory and possible alternatives following the step-by-step procedure.

1. Data entry, presentation of analysis and selection of rate-limited and saturated datapoints

For each datapoint of the four response curves, *PPFD*, *A*, C_i, and *Y(II)* are entered as the outputs from IRGA software (or, when appropriate, corrected for CO_2 diffusion, see example below) in Sheet 1. The datasets are automatically plotted graphically below the tables. A colour code is maintained throughout the EFT: brown is used to indicate ambient O_2 conditions, blue refers to low O_2, modelled functions appear as continuous lines, modelled points appear as crosses, grey cells contain general output and white cells require data input. The data entered in Sheet 1 will be automatically transferred to subsequent sheets in cells with a light-shaded background: for the sake of flexibility these cells can be overwritten by the user (see also 'Partial datasets' below), but in this case a copy of the original workbook needs to be saved to preserve the original functionality.

Along with each datapoint, a limitation code (1, 2 or 3) is required, which identifies the datapoints to be used in subsequent analyses and manipulations. Automatic routines for the limitation selection generally require dedicated software and have been tested only for A/C_i curve data selection (Gu *et al.*, 2010)) under ambient O_2. Given the complexity of the EFT and the necessity to deal with 3 (or more) limitations in each of 4 curves we implemented a simpler manual selection, in-line with Sharkey *et al.* (2007), that allows maximum transparency of the fitting procedures and straight-forward adjustments. For light-curves, '1' is assigned to the initial light-limited points (e.g. *PPFD* < 150 μmol m^{-2} s^{-1}); '2' to the light-limited points (e.g. *PPFD* < 500 μmol m^{-2} s^{-1}); and '3' to the remainder of the points. For A/C_i curves '1' is assigned to the initial Rubisco-limited part of the curve (e.g. C_i < 150 μmol mol^{-1}); '2' to the Rubisco-limited part of the curve (generally obtained under sub-ambient external CO_2 concentration, e.g. C_a < 400 μmol mol^{-1}); and '3' to the ribulose regeneration limited part of the curve (generally obtained under above-ambient external CO_2 concentration, e.g. C_a > 400 μmol mol^{-1}). Fitting steps are largely independent, meaning limitations can be adjusted between one step and the next. Individual datapoints can be excluded from further analysis (see instructions in Sheet 1).

2. Estimating Respiration in the light (R$_{LIGHT}$)

For the sake of this work 'Respiration' is primarily mitochondrial CO_2 release. Respiration in the light (R_{LIGHT}) is very difficult to resolve because of concurrent photosynthetic CO_2 uptake and photorespiratory CO_2 release under illumination.

All methods to estimate R_{LIGHT} involve assumptions. The simplest assumption is a relationship with R_{DARK}, which is easily measured, for instance $R_{LIGHT}=R_{DARK}$ [e.g. Kromdijk *et al.* (2010)], or, following the observation that respiration is down-regulated in the light, $R_{LIGHT}=0.5R_{DARK}$ [e.g. Martins *et al.* (2013)]. Because the magnitude of the down-regulation will depend on the species and environmental conditions (Buckley & Adams, 2011, Gandin *et al.*, 2014, Tcherkez *et al.*, 2008), these simple assumptions should be used with caution.

The method developed by Laisk (1977) [described in Brooks and Farquhar (1985), e.g. applied in Flexas *et al.* (2007)] identifies R_{LIGHT} as the *y*-value of the intersection of ≥2 linear A/C_i relationships assessed at limiting *PPFD*. The Laisk method assumes that R_{LIGHT} is not affected by *PPFD*, requires dedicated experimental routines, and because it mathematically underestimates R_{LIGHT}, has been deemed inadequate (Gu & Sun, 2014). An interesting simplification method, although based on the same theoretical construct, was presented by Brooks and Farquhar [(1985) hereafter BF method]. In the BF method, the *y*-value of a single linear A/C_i regression ($C_i \leq 150$ µmol mol^{-1}) in correspondence of $x = C_i*$ is taken as R_{LIGHT}. C_i*, the C_i–GA compensation point is generally assumed to equal $\Gamma*$, the C_C–GA compensation point (the C_C at which GA is zero), where $\Gamma*$ is derived from *in vitro* Rubisco specificity (see Step 11). Interestingly, when R_{LIGHT} values derived from the BF method are used for A/C_i modelling under the same *PPFD*, the independence of R_{LIGHT} on *PPFD* does not need to be assumed. We note that the mathematical underestimation theoretically highlighted by Gu & Sun (2014) is largely outweighed by artefacts dependent on CO_2 diffusion through the IRGA cuvette gaskets (see Supporting information Note 1) and this effect has previously resulted in considerable measurement artefacts (Drake *et al.*, 1997, Gu & Sun, 2014, Long & Bernacchi, 2003). For these reasons, the use of both the BF and Laisk methods should be discouraged with small IRGA chambers.

Alternatively, R_{LIGHT} can be estimated from light-response data, with the benefit of using measurements taken under a CO_2 concentration close to ambient or external to the cuvette (typically $400 - 550$ µmol mol^{-1}). The earliest method of Kok estimated R_{LIGHT} as the *y*-intercept of a linear regression between *A* and *PPFD*. A very limited portion of the light-curve can be used because linearity is soon lost (e.g. *PPFD* > 100 µmol photons m^{-2} s^{-1}) and the initial part has to be discarded [it has a different slope: the 'Kok effect' (Kok, 1948), see for review and examples Yin *et al.* (2009) and Yin *et al.* (2011a)]. The Kok method has recently been developed by Yin *et al.* (2011a) in a gas exchange-fluorescence method which corrects for non-linearity using chlorophyll fluorescence data: *A* is plotted against ¼ *Y(II) PPFD* yielding a linear relationship in a wider data range (e.g. < 300 µmol photons m^{-2} s^{-1}). Following this approach, in Sheet 2, R_{LIGHT} is independently estimated under low and ambient O_2 as the *y*-intercept of the fitted line:

$$A = s \, ¼ \, Y(II) \, PPFD \, - R_{LIGHT} \qquad\qquad 1$$

where *s* is a lumped conversion coefficient (see Step 6).

Eqn 1 is valid under non-photorespiratory conditions [an expression analogous to Eqn 1 can be derived for photorespiratory conditions see Eqn 7a in Yin *et al.* (2009), and Yin *et al.* (2014)]. This gas exchange-chlorophyll fluorescence method has been theoretically demonstrated (Yin *et al.*,

2004) and experimentally validated for C_3 and C_4 plants (Bellasio & Griffiths, 2014b, Yin *et al.*, 2009, Yin *et al.*, 2011a). Note that the estimate for R_{LIGHT} is obtained under low *PPFD* and the independence of R_{LIGHT} from *PPFD* is assumed. The derivation of R_{LIGHT} in Sheet 2 was separated from the derivation of *s* in Sheet 6a to allow additional features in Sheet 2, including the possibility to add additional data to the regressions (the light-limited part of the A/C_i curve and R_{DARK}, measured under ambient and/or low O_2); and the possibility to fit a value for R_{LIGHT} concurrently to ambient and low O_2 data, since in practical terms, any O_2 effect may be considered negligible (Yin *et al.*, 2009). Results can be compared with the BF method in the additional features embedded in Sheet 11.

3. Initial photochemical yield of PSII, *Y(II)*LL

*Y(II)*LL represents the initial (and maximal) photochemical yield of PSII obtained under conditions of steady state illumination and accounts for conversion losses occurring under operational conditions. Based on the observation that *Y(II)* increases monotonically at decreasing *PPFD* (Yin *et al.*, 2014), Sheet 3 calculates *Y(II)*LL as the *y*-intercept of a function fitted to *Y(II)* plotted against *PPFD*. In Sheet 3 a straight line is fitted to the initial light-limited portion of the light-response curve, and additional features in Sheet 3 allow comparison with quadratic and exponential functions fitted to any combination of datapoints. F_V/F_M [*Y(II)* measured on dark-adapted leaves, (Baker, 2008, Maxwell & Johnson, 2000)] does not reflect PSII operational conditions under illumination (Schansker *et al.*, 2014, Stirbet & Govindjee, 2011) and therefore F_V/F_M is not a good proxy for *Y(II)*LL (Yin *et al.*, 2014).

4. Light dependence of gross assimilation (GA), light-saturated gross assimilation (GA*SAT*), initial quantum yield for CO_2 fixation (Y(CO2)*LL*), and PPFD–A compensation point (LCP)

The dependence of *GA* on *PPFD* can be modelled empirically. The derived parameters are informative, but no longer used in predictive modelling having been surpassed by mechanistic predictions based on *J* (von Caemmerer, 2013, Yin & Struik, 2009a). In sheets 4a and 4b we modified an equation from Prioul and Chartier (1977) to empirically describe *GA* as:

$$GA_{MOD} = \frac{Y(CO_2)_{LL}\,PPFD + GA_{SAT} - \sqrt{(Y(CO_2)_{LL}\,PPFD + GA_{SAT})^2 - 4\,m\,Y(CO_2)_{LL}\,PPFD\,GA_{SAT}}}{2\,m} \qquad 2$$

Eqn 2 is a non-rectangular hyperbola parameterised by GA_{SAT}, *Y(CO2)*LL and *m,* an empirical factor ($0 \leq m \leq 1$) defining the curvature. GA_{SAT} defines the horizontal asymptote ($GA=GA_{SAT}$) and represents the light-saturated rate of *GA* under the CO_2 concentration used for measurements.

$Y(CO_2)_{LL}$ corresponds to the maximal quantum yield for CO_2 fixation ($Y(CO_2)$ i.e. the conversion efficiency of $PPFD$ into fixed CO_2, often referred to as Φ_{CO2}) under the CO_2 concentration used for measurements, and defines the inclined asymptote ($GA=Y(CO_2)_{LL} PPFD$). To facilitate the physiological interpretation of m, Sheet 4 calculates the $PPFD$ which half saturates GA ($PPFD_{50}$), analogous to a $K_{1/2}$ kinetic parameter. The values of $Y(CO_2)_{LL}$, m and GA_{SAT} are found by iterative fitting of GA_{MOD} to GA. A recently proposed linear alternative for the derivation of $Y(CO_2)_{LL}$ (Yin *et al.*, 2014) can be compared in the additional features of Sheet 6a. From Sheet 4a onwards we included the possibility to log-transform residuals. By partially correcting for proportionality between residuals and GA, this feature increases the weight of initial datapoints (e.g. low $PPFD$) in determining the characteristics of the fitted curve. The opportunity to log-transform depends on the structure of the dataset and the characteristics of error and should be considered on a case-by-case basis.

The fitted hyperbola is used to calculate the $PPFD$–A compensation point (LCP, i.e. the $PPFD$ at which A is zero). The LCP is a versatile index expressing the metabolic cost of basal metabolism, related to the degree of shade acclimation or adaptation (Timm *et al.*, 2002, Walters & Reich, 1996) and represents the capacity of crops to perform well under limited light (Bellasio & Griffiths, 2014a, Craine & Reich, 2005, Yongjian *et al.*, 1998). Stress events affecting respiration or the photosynthetic capacity will readily be mirrored by the LCP [e.g. Yongjian *et al.* (1998)]. The LCP is easily determined and, since it relies on light-response data and is generally measured under external CO_2 concentration, is inherently more accurate than the C_i–A compensation point Γ. Sheets 4a and 4b calculate the LCP by solving Eqn 2 for $PPFD$ under the condition of $A=0$, i.e. $GA=R_{LIGHT}$:

$$LCP = \frac{GA_{SAT}R_{LIGHT} - mR_{LIGHT}{}^2}{Y(CO_2)_{LL}\, GA_{SAT} - Y(CO_2)_{LL}R_{LIGHT}} \qquad 3$$

A linear alternative to derive LCP from the initial region of the light-response curve can be compared in the additional features of Sheet 3.

5. CO_2 dependence of assimilation (A), CO_2-saturated assimilation (A$_{SAT}$), initial carboxylating efficiency for CO_2 fixation (CE), C_i–A (Γ) and C_i–GA (C$_i$*) compensation points

The relationship between A and C_i can be modelled mechanistically to derive Rubisco CO_2-saturated rate of carboxylation (Step 13), however, important information can also be acquired by empirical modelling without the need for any particular physiological constraint. Farquhar and Sharkey (1982) mathematically described the initial part of the A/C_i curve with a linear relationship between A and C_i as $A=CE (C_i\text{-}\Gamma)$, where Γ is the C_i–A compensation point. It has been noted that

9

the relationship between A and C_i is never linear, even at very low C_i (Gu & Sun, 2014). To account for this physiological non-linearity and to avoid arbitrary selection of the part of the curve considered linear (selection of cut-off point), we propose that A should be modelled in terms of C_i through a non-rectangular hyperbola (analogous to Eqn 2):

$$A_{MOD} = \frac{CE\,(C_i - \Gamma) + A_{SAT} - \sqrt{(CE\,(C_i - \Gamma) + A_{SAT})^2 - 4\,\omega\,CE\,(C_i - \Gamma)\,A_{SAT}}}{2\,\omega} \qquad 4$$

Eqn 4 is calculated in sheets 5a and 5b and is parameterised by A_{SAT}, CE, Γ and ω. A_{SAT} represents the CO_2-saturated rate of A under the *PPFD* of the measurement, and is the horizontal asymptote ($A=A_{SAT}$). CE is the maximal carboxylating efficiency for CO_2 fixation (CE), and defines the inclined asymptote, which has the equation $A=CE\,(C_i-\Gamma)$, i.e. the asymptote equation corresponds to the linear equation of Farquhar and Sharkey (1982). ω is an empirical factor ($0\leq \omega \leq 1$) defining the curvature. To facilitate the physiological interpretation of ω, sheets 5a and 5b calculate the C_i which half saturates A (C_{i50}) – analogous to a $K_{1/2}$ kinetic parameter. With R_{LIGHT} derived in Step 2, the values of CE, ω, Γ, and A_{SAT} are found by iterative fitting of A_{MOD} to measured A. Eqn 4 can be used for all assimilatory physiologies, meaning CE, ω, Γ, and A_{SAT}, which describe the A/C_i response, can diagnose enhanced or disrupted photosynthetic traits (see 'Intermediate and Engineered assimilatory pathways', below).

The fitted Eqn 4 can be useful to assess stomatal limitation (L_S) imposed by stomatal conductance (g_S) in analogy with the graphical method (Farquhar & Sharkey, 1982, Long & Bernacchi, 2003). Stomatal limitation L_S is generally assessed by comparing a value of assimilation rate A' measured under ambient CO_2 concentration (i.e. when $C_i = C_a - \frac{A}{g_S}$) with the hypothetical A'' that would be obtained if the mesophyll had free access to the CO_2 in the ambient air (i.e. when $C_i=C_a$). For additional flexibility in Sheet 5a C_a and C_i can be specified so that stomatal limitation can be calculated under ambient or any other CO_2 concentration. Sheet 5a calculates L_S as $L_S = \frac{A''-A'}{A''}$, where A' is calculated by solving Eqn 4 for the specified C_i and A'' is calculated solving Eqn 4 for the specified C_a.

If a value for R_{LIGHT} is available, sheets 5a and 5b calculate the C_i–GA compensation point C_i^* (also referred to as the CO_2 compensation point in absence of R_{LIGHT}). C_i^* is a useful proxy in comparative studies, having the advantage over Γ of not being susceptible to variability in R_{LIGHT} which responds readily to environmental conditions (Bellasio & Griffiths, 2014a, Bellasio & Griffiths, 2014b, Buckley & Adams, 2011). C_i^* is solved in sheets 5a and 5b as the x-value of the fitted Eqn 4 in correspondence with $A_{MOD}=-R_{LIGHT}$ (Ethier & Livingston, 2004), similarly to Eqn 3.

$$C_i^* = \Gamma - \frac{\omega R_{\text{LIGHT}}^2 + A_{\text{SAT}} R_{\text{LIGHT}}}{CE\,A_{\text{SAT}} + CE\,R_{\text{LIGHT}}} \qquad\qquad 5$$

The rate of triose phosphate use (TPU) can be calculated directly from *GA* under conditions of TPU limitation (when A is saturated, or decreases, under increasing CO_2). Such a condition is most frequently encountered under high C_i and low O_2 partial pressures (see Figure 1), but can be observed under ambient O_2 (Sharkey *et al.*, 2007). Sheet 5a 5b calculate TPU as TPU = GA/3 (Harley & Sharkey, 1991), using a selection of appropriate datapoints at the high C_i end of the *A/C_i* curve to initially derive *GA*.

6. Fraction of PPFD harvested by PSII: Valentini and Yin calibrations

The fraction of *PPFD* harvested by PSII is used to calculate *J,* and it is derived for each individual plant using the data obtained under low O_2 conditions (see 'Measurements and rationale for different O_2 levels' above). Two calibration approaches have been proposed: the mechanistic approach of Yin (Yin *et al.*, 2009, Yin *et al.*, 2004) and the empirical approach of Valentini (Valentini *et al.*, 1995).

The Yin approach is based on the linear relationship between *A* and ¼ *Y(II) PPFD* (Eqn 1) of which the *y*-intercept, R_{LIGHT}, was derived in Sheet 3. In Sheet 6a, the slope *s* is derived. *s* is a conversion coefficient lumping the fraction of *PPFD* harvested by PSII with several other difficult to measure quantities (Yin *et al.*, 2004), which depend on leaf absorptance, PSII optical cross-section, alternative electron pathways and engagement of cyclic electron flow (Yin *et al.*, 2009).

Alternatively, in Sheet 6b the approach of Valentini fits an empirical linear relationship between *Y(CO₂)* and *Y(II)*:

$$Y(II) = k\,Y(CO_2) + b \qquad\qquad 6$$

where *Y(II)* is measured directly and *Y(CO₂)* is calculated as $\frac{GA}{PPFD}$, *k* is the slope and *b* is the intercept of the fitted line. *b* represents the fraction of *Y(II)* not used by RPP + PCO cycles. The fraction of *PPFD* harvested by PSII (αβ) is calculated as αβ=4/*k*.

In many applications following the approach described in (von Caemmerer, 2000), a calibration factor was derived as leaf absorptance × PSII optical cross-section, where leaf absorptance may be measured, and the PSII optical cross-section is generally assumed (0.45 – 0.5). Negligible engagement of alternative sinks and cyclic electron flow are also implicitly assumed (von

11

Caemmerer, 2000, von Caemmerer, 2013, Yin *et al.*, 2004). These assumptions and simplifications introduce uncertainties and errors, particularly if the same calibration factor is used for plants from contrasting treatments (light quality changes chloroplast orientation, drought influences leaf reflectance, high *PPFD* may result in the engagement of alternative sinks, etc.).

*7. Initial quantum yield for electron transport J (*Y(J)$_{LL}$*)*

The initial quantum yield for electron transport ($Y(J)_{LL}$) is the maximal conversion efficiency of *PPFD* into *J* measured under limiting light ('K_{2LL}' in the notation of Yin). In principle $Y(J)_{LL}$ could be derived as the initial slope of the curve describing the *PPFD* dependence of *J* (see Step 9), however, in line with Yin *et al.* (2014) and Yin *et al.* (2009), we found it more reliable to derive $Y(J)_{LL}$ separately. In Sheet 6a with the calibration of Yin $Y(J)_{LL}$ is calculated as:

$$Y(J)_{LL} = s\, Y(II)_{LL} \qquad\qquad 7$$

In Sheet 6b $Y(II)_{LL}$ is calculated using the calibration of Valentini:

$$Y(J)_{LL} = \alpha\beta\,(Y(II)_{LL} - b) \qquad\qquad 8$$

Eqn 7 and 8 are entirely based on data obtained during experimentation, and because they do not rely on assumptions or external parameterisation, are of general applicability.

$Y(J)_{LL}$ should be independent of background O_2 concentration but it varies between different plants. In many applications following the approach of Farquhar *et al.* (1980) $Y(J)_{LL}$ is not explicit, but calculated as: leaf absorptance$\times\frac{1}{2}(1\text{-}f)$, where leaf absorptance may be measured, $\frac{1}{2}$ is the assumed PSII optical cross-section (see Step 6) and *f* is an empirical correction factor (0.85) (Evans, 1987, Farquhar *et al.*, 1980, von Caemmerer, 2000). As noted in 6, invariant values may bias comparative studies.

*8. Electron Transport Rate (*J*)*

The importance of determining *J* accurately cannot be overstated (Martins *et al.*, 2013) because further derivations (rates of photorespiration and carboxylation, mesophyll conductance to CO_2 diffusion see Eqn 13, 14, 18, 19) assume that *J* is entirely partitioned between RPP and PCO cycles, without accounting for any 'overflow' diverted to alternative sinks. There are various formulations for calculating *J* (Bellasio & Griffiths, 2014b, Valentini *et al.*, 1995, von Caemmerer, 2000, Yin *et*

al., 2004). We implemented three approaches that can be selected depending on the particular modelling requirements.

Firstly, following the approach of Yin, sheets 8, 9, 10 and 12 calculate *J* as:

$$J = s\,Y(II)\,PPFD \qquad\qquad 9$$

Alternatively, following the approach of Valentini, sheets 8, 9, 10 and 12 calculate *J* as:

$$J = \alpha\beta\,(Y(II) - b)\,PPFD \qquad\qquad 10$$

where parameters were previously defined.

Although Eqn 9 and 10 inherently differ they have often been considered equivalent. Eqn 9 compares to 'the potential rate of electron transport' in the notation of Farquhar (Buckley & Adams, 2011, Farquhar *et al.*, 1980)], includes 'additional PET' ['PETa' in the notation of Yin *et al.* (2009)], which is the fraction of *J* used by RPP and PCO under limiting *PPFD* that gets diverted to alternative sinks under high *PPFD*. Conversely Eqn 10 is corrected by the parameter *b*, and does therefore not include the electron demand by alternative sinks. It is comparable with 'the actual rate of electron transport' in the notation of Farquhar (Buckley & Adams, 2011, Farquhar *et al.*, 1980). The difference is negligible under limiting *PPFD*, but, under moderate or high *PPFD*, the Yin approach tends to overestimate *J* as we defined it in 'Measurements and rationale for different O_2 levels', and Eqn 10 is generally preferred [e.g. (Flexas *et al.*, 2007, Flexas *et al.*, 2006, Long & Bernacchi, 2003)]. Eqn 9 and 10 are underpinned by three assumptions: 1) R_{LIGHT} does not vary much with light level; 2) if triose phosphate utilisation is limiting, it is entirely mirrored by feedback on *Y(II)*; and 3) *s*, αβ and *b* are constant, that is, the degree of engagement of alternative sinks and cyclic electron flow do not vary with *PPFD*. Of these, in line with (Martins *et al.*, 2013), we highlight how (3) is the most critical. In fact, deviations from linearity have been reported for both the Yin and Valentini approaches in C_3 and C_4 plants (Bellasio & Griffiths, 2014b, Gilbert *et al.*, 2012). These may depend on the differential engagement of alternative sinks, or biases introduced by sub-saturating flash intensities (Harbinson, 2013). Further, we add that any vertical difference in *Y(II)* quenching down the leaf profile, caused either by changes in light intensity (Terashima *et al.*, 2009) or light quality (Bellasio & Griffiths, 2014c) will similarly affect linearity [C.B. unpublished analysis from (Bellasio & Griffiths, 2014c) data].

Both the Valentini calibration (Gilbert *et al.*, 2012) and the Yin calibration (Bellasio & Griffiths, 2014b) were modified to account for non-linearity, and here we implemented the simple approach

13

presented by Bellasio (Bellasio & Griffiths, 2014a, Bellasio & Griffiths, 2014b) in the experimentally validated C_3 version (Bellasio *et al.*, 2014). sheets 8, 9, 10, and 12 calculate *J* for each point of the light and *A/C*i curve as:

$$J = 4\,GA_{\text{LOW}}\frac{Y(II)_{\text{AMB}}}{Y(II)_{\text{LOW}}} \qquad\qquad 11$$

where $Y(II)_{\text{AMB}}$ and $Y(II)_{\text{LOW}}$ are the values of *Y(II)* measured under ambient and low O_2, respectively. Eqn 11 relies on assumptions (1) and (2), but not on (3) and it can therefore be used flexibly, however, Eqn 11 is experimentally more demanding than Eqn 9 and 10 in terms of precision of *Y(II)* (experimental noise is not statistically smoothed), and the number of required datapoints (the PPFD and CO_2 levels need to be symmetrical under low and ambient O_2).

9. PPFD dependence of J

The process of photosynthetic electron transport is driven by light and displays a saturating response to increasing *PPFD*. Although some of the processes responsible for the saturation kinetics are known (e.g. non photochemical quenching), the light dependence of *J* is generally described empirically by a non-rectangular hyperbola analogous to Eqn 2 (Farquhar & Wong, 1984), implemented in Sheet 9:

$$J_{\text{MOD}} = \frac{Y(J)_{\text{LL}}\,PPFD + J_{\text{SAT}} - \sqrt{(Y(J)_{\text{LL}}\,PPFD + J_{\text{SAT}})^2 - 4\theta J_{\text{SAT}}Y(J)_{\text{LL}}\,PPFD}}{2\theta} \qquad 12$$

Eqn 12 describes the relationship between J_{MOD} and *PPFD* in terms of J_{SAT}, $Y(J)_{\text{LL}}$ and θ. J_{SAT} (J_{MAX} in the notation of Farquhar) represents the value of *J* under infinite *PPFD* and defines the horizontal asymptote ($J_{\text{MOD}}=J_{\text{SAT}}$). $Y(J)_{\text{LL}}$ represents the initial (and maximal) quantum yield for electron transport, defining the inclined asymptote ($J_{\text{MOD}}= Y(J)_{\text{LL}}\,PPFD$). θ is an empirical factor ($0\le \theta \le 1$) defining the curvature. To facilitate the physiological interpretation of θ, Sheet 9 calculates the *PPFD* which half saturates J_{MOD} ($PPFD_{50}$) in analogy to a kinetic parameter $K_{1/2}$. With $Y(J)_{\text{LL}}$ found in Step 7, J_{SAT} and θ are derived in Sheet 9 by fitting J_{MOD} (Eqn 12) to empirical values of *J* (Eqn 9, 10 or 11) calculated at each *PPFD*. This operation is limited to ambient O_2, because under low O_2, by assuming non-photorespiratory conditions, $J_{\text{MOD}} = 4\,GA_{\text{MOD}}$, $Y(J)_{\text{LL}} \approx 4$ $Y(CO_2)_{\text{LL}}$, $J_{\text{SAT}} \approx 4\,GA_{\text{SAT}}$ (quantities derived in Sheet 4b).

$Y(J)_{\text{LL}}$, J_{SAT} and θ are commonly used in predictive modelling to estimate *J* under a given *PPFD*. Buckley and Diaz-Espejo (2014) recently highlighted the differences between J_{SAT} and the value of

J derived in the Sharkey fitting tool (Sharkey *et al.*, 2007). While J_{SAT} is mathematically extrapolated to infinite *PPFD*, J (Sharkey) is a CO_2-saturated value found under a particular *PPFD* used for the data collection (e.g. 1500 μmol m^{-2} s^{-1}, for comparison J values appear in Sheet 10). J_{SAT} is particularly suitable for predictive purposes which relate to a specific CO_2 concentration (e.g. ambient CO_2), although, in principle, J_{SAT} should be independent of CO_2 concentration (Farquhar *et al.*, 1980). In addition J_{SAT} does not mathematically bias predictive models unlike when values of J derived under a finite *PPFD* level are used (Buckley & Diaz-Espejo, 2014).

*10. Photorespiratory CO_2 release (*F*), Rubisco rate of Carboxylation (*V_C*) and Oxygenation (*V_O*)*

V_O and V_C cannot be measured directly, but can be resolved from J and GA under the assumption that NADPH is entirely used by the RPP and PCO cycles. Knowing that: 1) the RPP cycle requires 2 NADPH per each Rubisco carboxylase event; 2) the PCO cycle requires 2 NADPH per each oxygenase event [1 NADPH for the reduction of the PGA directly produced by Rubisco, 0.5 NADPH to recycle glycolate and 0.5 NADPH to reduce the PGA regenerated (Bellasio *et al.*, 2014, Bellasio & Griffiths, 2014c, von Caemmerer, 2000)]; and 3) two electrons are carried per NADPH, Sheet 10 calculates V_O as [for derivation see Bellasio *et al.* (2014)]:

$$V_O = \tfrac{1}{6}J - \tfrac{2}{3}GA \qquad\qquad 13$$

Where J can be derived alternatively with Eqn 9, 10 or 11. Sheet 10 calculates V_C from the leaf mass balance as:

$$V_C = GA + \tfrac{1}{2}V_O \qquad\qquad 14$$

And the rate of photorespiratory CO_2 release, or photorespiration rate (F) as $F = \tfrac{1}{2}V_O$.

Sheet 10 calculates Eqn 13 and 14 for each point of the light and A/C_i curves under ambient O_2. Under low O_2, by assuming non-photorespiratory conditions, V_O and F are zero and $V_C=GA$.

Since the NADPH requirements and the overall CO_2 mass balance are the same for all pathways of carbon assimilation (Bellasio *et al.*, 2014, von Caemmerer, 2013), Eqn 13 and 14 are universally valid and can be used to screen disrupted or manipulated photosynthetic phenotypes (see 'Intermediate and Engineered assimilatory pathways', below). Regarding experimental conditions, it is appropriate to limit the application of Eqn 13 and 14 within a valid range of s or αβ, however, if V_O, V_C, and F are desired for different conditions (e.g. lower temperature) s or αβ can be recalibrated with a point-measurement under low O_2 (Bellasio *et al.*, 2014).

11. Rubisco specificity factor $S_{C/O}$

Rubisco specificity combines the maximum reaction rates and the affinity for the substrates CO_2 and O_2, and it is defined as [Eqn A3 in (von Caemmerer, 2013)]:

$$S_{C/O} = \frac{V_{OMAX}K_C}{V_{CMAX}K_O} \qquad 15$$

Where V_{OMAX} is the O_2-saturated oxygenation rate, K_C is the Michaelis-Menten constant for carboxylation, V_{CMAX} is the CO_2-saturated carboxylation rate and K_O is the Michaelis-Menten constant for oxygenation. $S_{C/O}$ was suggested to vary across species [e.g. (Delgado *et al.*, 1995, Parry *et al.*, 1989)] and environmental conditions (Galmés *et al.*, 2005) but some variation may be associated with methodological approaches. Accuracy of $S_{C/O}$ is critical because of the sensitivity of g_M to $S_{C/O}$. $S_{C/O}$ is often measured *in vitro* [e.g. Cousins *et al.* (2010)], conditions which are somewhat idealised and may differ from those at leaf-level (von Caemmerer, 2000). *In vitro* $S_{C/O}$ values are available only for a limited number of species, and since a rapid determination would benefit high throughput genotype screening (Carmo-Silva *et al.*, 2014), estimating $S_{C/O}$ from gas exchange measurements is highly desirable.

$S_{C/O}$ can be calculated from Γ^* (the C_c–GA compensation point) as $S_{C/O} = \frac{O}{2\Gamma^*}$ (where O is O_2 concentration at the carboxylating sites), however, the derivation of Γ^* requires g_M, which is still unknown at this step (see Table 1). In the work of Laisk (1977), described in Step 2, infinite g_M was assumed and Γ^* was calculated as $\Gamma^*=C_i^*$. Although under this assumption $S_{C/O}$ can be slightly misestimated (Gu & Sun, 2014), Galmés *et al.* (2006) confirmed the general validity of method: the $S_{C/O}$ estimates compared well with *in vitro* measurements in control plants and under mild stress (c. 5% difference).

The method of Yin *et al.* (2009) addresses the shortcomings of the Laisk method by deriving an actual C_C-based $S_{C/O}$ without requiring g_M, and has the additional benefit of being less susceptible to CO_2 diffusion (see supporting information Note 1 and 2). We implemented a non-linear upgrade of the Yin method in Sheet 11: assimilation is modelled under ambient O_2, A_{AMB} as a function of assimilation measured under low O_2, A_{LOW}, as:

$$A_{AMB} = (A_{LOW} + R_{LIGHT})\frac{CE_{AMB}}{CE_{LOW}} - \left(\frac{O_{AMB} - O_{LOW}}{2\,S_{C/O}} + C_{iLOW} - C_{iAMB}\right)CE_{AMB} - R_{LIGHT} \qquad 16$$

Where CE_{AMB} and CE_{LOW} are the initial slopes of the A/C_i curves under ambient and low O_2 determined non-linearly in Step 5. O_{AMB} and O_{LOW} are the ambient and low O_2 concentration at the site of carboxylation. With R_{LIGHT} estimated previously, A_{LOW}, C_{iLOW} (C_i values measured under low O_2), and C_{iAMB} (C_i value measured under ambient O_2) measured by gas exchange, Sheet 11 finds $S_{C/O}$ by fitting A_{AMB} to A.

Bearing in mind that Galmés *et al.* (2006) reported major errors in estimating $S_{C/O}$ from severely stressed plants and in line with the recommendations of Yin *et al.* (2009), it is appropriate to estimate $S_{C/O}$ on an adequate number of control (or healthy) plants and then average across them to retrieve a single estimate of $S_{C/O}$ which may then be used in subsequent modelling steps. Note that the EFT allows values of $S_{C/O}$ to be overwritten (see instructions in the EFT), so that *in vitro* values can be added if preferred.

For comparison, the original linear method of Yin *et al.* (2009) (CE_{AMB} CE_{LOW} are determined by linear fitting to the initial portion of A/C_i curves), is implemented as an additional feature in Sheet 11 (but see the shortcomings highlighted in Step 5). Further, in the additional features of Sheet 5a, $S_{C/O}$ is calculated using the Laisk approach, using the non-linear C_i^* values from step 5.

12. Mesophyll conductance to CO_2 diffusion (g_M)

Photosynthetic CO_2 fixation (A), results in the depletion of [CO_2] in the vicinity of Rubisco located in the chloroplast stroma, thus driving a CO_2 concentration gradient between the substomatal cavity and carboxylating sites C_i-C_C (Evans *et al.*, 2009, Evans & Loreto, 2000, Evans & von Caemmerer, 1996, Parkhurst & Mott, 1990). The diffusion path comprises the intercellular air spaces, the liquid phase, the cell walls, the plasmalemma, the cytosol, the chloroplast envelope and finally the stroma (Tholen *et al.*, 2012b, Tholen & Zhu, 2011). The overall ability to conduct CO_2 through this path is mathematically expressed as the mesophyll conductance:

$$g_M = \frac{A}{C_i - C_C} \qquad 17$$

Despite the complexity of CO_2 diffusion, for simplicity, early reports assumed infinite g_M (Farquhar *et al.*, 1980), but it is clear that g_M has a finite value and co-limits A together with stomatal conductance over a wide range of environmental conditions (Flexas *et al.*, 2012, Flexas *et al.*, 2009, Niinemets *et al.*, 2009a, Niinemets *et al.*, 2009b). g_M depends on anatomical traits, such as cell wall thickness, chloroplast distribution, surface area of cells (Terashima *et al.*, 2011), and biochemical traits, such as the activity of carbonic anhydrases or aquaporins (Heckwolf *et al.*, 2011). In addition, environmental factors, such as CO_2 concentration, temperature, *PPFD*, nutrient availability and stress (Flexas *et al.*, 2012) are known to affect g_M. Remarkably, g_M (as defined

above and expressed by Eqn 17) is a flux-weighted quantity and depends on V_O/V_C: an increased rate of photorespiration lowers g_M even if the physical resistances in the diffusion pathway do not change (Tholen *et al.*, 2014, Tholen *et al.*, 2012b). We distinguish two types of variability which are relevant for data analysis: a component of g_M which does not change during the gas exchange experiment (e.g. as affected by N level), and a component of g_M which does change during the gas exchange experiment [e.g. as affected by V_O/V_C; for recent review see (Flexas *et al.*, 2008, Tholen *et al.*, 2012b, Warren, 2006)].

Detecting short-term variations requires that g_M be resolved for each datapoint (hereafter defined as the point approach). The theoretical framework has been described by (Harley *et al.*, 1992): if $S_{C/O}$ is known, C_C can be calculated from V_O/V_C as $C_C = \frac{O}{S_{C/O}\frac{V_O}{V_C}}$ (where $\frac{V_O}{V_C} = \frac{\text{Eqn } 13}{\text{Eqn } 14}$), then g_M is resolved by Eqn 17, or, in the equivalent notation of (Harley *et al.*, 1992):

$$g_M = \frac{A}{C_i - \frac{\Gamma^*(J+8GA)}{J-4GA}} \qquad\qquad 18$$

Sheet 12 calculates Eqn 18 for each light-limited datapoint. Because experimental noise (Evans, 2009, Gilbert *et al.*, 2012, Gu & Sun, 2014, Pons *et al.*, 2009) and true g_M variability may co-occur, Eqn 18 often yields unrealistic g_M values, which have to be filtered out using arbitrary criteria (Harley *et al.*, 1992, Martins *et al.*, 2013). Furthermore, systematic patterns of g_M variation and biases are generated solely as a consequence of error in the estimation of input parameters (Gilbert *et al.*, 2012, Gu & Sun, 2014). As a result, the magnitude of true g_M variability is still debated and a conclusive theoretical interpretation remains lacking (Buckley & Warren, 2014, Gu & Sun, 2014, Tholen *et al.*, 2012b). For these reasons, it is probably not appropriate to study the instantaneous response of g_M through Eqn 18, while it is more productive to limit the use of gas exchange-fluorescence data to resolving long term effects (Gu & Sun, 2014).

Long-term effects on g_M (e.g. the influence of anatomical and stable biochemical traits) are not affected by the gas exchange routine, and can be resolved by averaging g_M over the course of the experiment. The availability of values of J for all datapoints allows the variable J method (Harley *et al.*, 1992), to be used in Sheet 12, including a recent refinement by (Yin *et al.*, 2009). We adopted the special case where g_M is constant for the duration of gas exchange measurements ($\delta=0$ in Yin's notation), Eqn 12 in Yin *et al.* (2009), simplifies to the equation derived by von Caemmerer and Evans (1991), see Eqn A23 in von Caemmerer (2013):

$$A_{\mathrm{J}} = \frac{(C_{\mathrm{i}} + 2\Gamma^*)g_{\mathrm{M}} + \frac{J}{4} - R_{\mathrm{LIGHT}} - \sqrt{\left[(C_{\mathrm{i}} + 2\Gamma^*)g_{\mathrm{M}} + \frac{J}{4} - R_{\mathrm{LIGHT}}\right]^2 - 4g_{\mathrm{M}}\left[(C_{\mathrm{i}} - \Gamma^*)\frac{J}{4} - R_{\mathrm{LIGHT}}(C_{\mathrm{i}} + 2\Gamma^*)\right]}}{2}$$

Eqn 19 models A with C_i measured by gas exchange, Γ^* derived from $S_{\mathrm{C/O}}$ (Step 11), J calculated with either Eqn 9, 10 or 11 (Step 8) and R_{LIGHT} estimated in Step 2. Sheet 12 finds g_{M} by iteratively fitting A_{J} to A. In this way the experimental noise is statistically smoothed without losing information and a wide portion of the dataset can be included in the curve-fitting. In selecting the points to include in the fitting procedure it has to be noted that Eqn 19 is valid whenever J mirrors the reducing power demand for RPP + PCO cycles, that is, whenever V_{O} and V_{C} fully feedback on *Y(II)*. This condition is generally satisfied (even under low C_i, see the plot of *Y(II) / Y(CO₂)* in Sheet 6b, and when TPU regeneration is limiting photosynthesis, see Figure 1 and the example below). Although it is not advisable to fit low C_i data (Gilbert *et al.*, 2012, Gu & Sun, 2014), points spanning ambient C_a, and light-curve data, may be fitted (Yin *et al.*, 2009, Yin & Struik, 2009b). These datapoints are less prone to the issue of CO_2 diffusion in small IRGA chambers (see Supporting information Note 1) and will improve the reliability of the g_{M} estimate. The selection of the fitted data will influence g_{M}, because, as noted above, g_{M} changes continuously between datapoints, and it is therefore critical to maintain consistency in experimental conditions (*PPFD* and C_a) and determine cut-off points beforehand in a pilot experiment.

The values of g_{M} found with this procedure may highlight manipulated leaf anatomy or disrupted photosynthetic phenotypes and will be useful to parameterise updated predictive models which take into account this important physiological trait (Sun *et al.*, 2014b).

13. *Rubisco kinetics* – In vivo *maximum carboxylation rate (*V_{CMAX}*) amd* in vivo *effective Michaelis-Menten constant for CO_2 [K$_C$(1+O/K$_O$)]*

A model to interpret leaf-level assimilation was initially developed by Farquhar *et al.* (1980), referred to as the FvCB model, and has since been refined (Ethier & Livingston, 2004, Gu *et al.*, 2010, von Caemmerer, 2013). Briefly, the FvCB is a mechanistic model based on the *in vitro* kinetics of fully-activated, RuBP-saturated Rubisco described in O_2-free media by a Michaelis-Menten type saturating response. Leaf-level processes are then incorporated (Ethier & Livingston, 2004). These include firstly, the competitive inhibition of O_2 on Rubisco catalytic activity, which increases the apparent Rubisco K_M; secondly, photorespiratory and respiratory CO_2 release, which introduce a finite compensation point; and finally, the effect of a finite g_{M}, which further changes the shape of the modelled function. The effect of limiting RuBP supply manifests at a threshold C_C value above which the equations for Rubisco-limited photosynthesis are no longer valid. RuBP-

limited (and, at higher C_i, also TPU-limited) datapoints are therefore excluded from this fitting by assigning a limitation > '2' [see Step 1, and Gu *et al.* (2010)].

Although all curve-fitting approaches from the literature use the FvCB model, several simplifications and assumptions are unavoidable due to the limited information available for individual plants. Of the complete FvCB model, as formulated by Ethier and Livingston, the only unknown parameters yet to derive by the EFT are V_{CMAX} and $K_C(1+O/K_O)$, which can be fitted concurrently in Step 13. As compared to traditional curve-fitting, this approach uses 1) the g_M value derived in Step 12, thereby eliminating a source of V_{CMAX} underestimation; 2) fits $K_C(1+O/K_O)$ for each individual plant; and 3) does not rely on literature values for Γ^*, instead using the value for C_i–A compensation point (Γ) empirically derived in Step 5, resulting in a better fit between A and A_C (Gu *et al.*, 2010). This approach has several benefits. Firstly, differences in photosynthetic capacity between plants are not uniquely attributed to differences in V_{CMAX}: leaves operating at the same C_i can achieve different A with different g_M or $K_C(1+O/K_O)$. Secondly, this method is less susceptible to errors introduced by treatments affecting g_M or $K_C(1+O/K_O)$ [e.g. stress (Ethier & Livingston, 2004)], and is therefore better for resolving effects on Rubisco enzymatic activity (Sun *et al.*, 2014a). In Sheet 13, A is expressed as a function of C_i (Ethier & Livingston, 2004) as:

$$A_C = \frac{-b + \sqrt{b^2 - 4ac}}{2a} \qquad\qquad 20$$

where $a = -\frac{1}{g_M}$; $b = \frac{(V_{CMAX} - R_{LIGHT})}{g_M} + C_i + K_C\left(1 + \frac{O}{K_O}\right)$; $c = -\frac{(V_{CMAX} - R_{LIGHT})}{C_i - \Gamma}$.

Eqn 20 is a non-rectangular hyperbola parameterised to g_M, V_{CMAX}, R_{LIGHT}, $K_C(1+O/K_O)$ and Γ. V_{CMAX} represents the horizontal asymptote ($GA=V_{CMAX}$); $K_C(1+O/K_O)$ defines the curvature and corresponds to the CO_2 concentration which half saturates GA; while Γ is the C_i–A compensation point. With C_i measured by gas exchange, R_{LIGHT}, Γ, and g_M derived in Sheet 5a), 3, and 12 respectively, V_{CMAX}, and $K_C(1+O/K_O)$ are found by fitting A_C to A. Methodological alternatives include the possibility of concurrently fitting g_M [similarly to the tool of Sharkey *et al.* (2007)], and/or Γ, and/or, if preferred, using literature values for $K_C(1+O/K_O)$ (see instructions in Sheet 13 and video tutorial).

In addition to fitting Eqn 20 to ambient O_2 A/C_i data (Sheet 13a), we propose Eqn 20 to be fitted to low O_2 A/C_i data (Sheet 13b). This procedure provides an independent estimate for V_{CMAX}, and $K_C(1+O/K_O)$, and can potentially ameliorate accuracy. These two estimates for V_{CMAX} can be reconciled in additional features of Sheet 13b (V_{CMAX} depends solely upon Rubisco characteristics and should not be affected by O_2 level) where a single V_{CMAX} value can be derived by concurrent fitting to ambient and low O_2 A/C_i data. K_C and K_O can be varied or set to literature values.

V_{CMAX}, and $K_C(1+O/K_O)$ can parameterise modern predictive models, but mathematical consistency has to be maintained: if predictive models implement an old formulation of the FvCB model (which for instance does not account for g_M), V_{CMAX}, and $K_C(1+O/K_O)$ have to be derived with a consistent set of equations. Further, here we have assumed that all datapoints assigned the limitation '1' and '2' are actually Rubisco-limited. If a more sophisticated selection of the cut-off point is desired, the routine of (Gu *et al.*, 2010) can be followed, perhaps inputting g_M, R_{LIGHT} and Γ^* derived from our EFT. Finally, consistency in the experimental routine between different plants is critical because too many low C_i levels and/or a slow acclimation routine can contribute to Rubisco inactivation, resulting in a linearization of the initial part of the A/C_i curve, and artefacts in deriving V_{CMAX} and $K_C(1+O/K_O)$ (Ethier & Livingston, 2004).

Adjusting for temperature

Fitted parameters strongly depend on temperature and are generally adjusted using empirical exponential functions [e.g.Sharkey *et al.* (2007)]. Here, because the EFT is self-contained, there is no need to reciprocally adjust parameters for temperature. However, if parameters are to be compared to fitted values measured at different temperatures, then temperature-adjustment should be undertaken (Bernacchi *et al.*, 2003, Bernacchi *et al.*, 2002, Bernacchi *et al.*, 2001, June *et al.*, 2004, Scafaro *et al.*, 2011, Yamori & von Caemmerer, 2009).

Partial datasets and use of the EFT

If datasets are incomplete due to unavoidable constraints on the original experimental design, or if re-analysing existing datasets, it is still possible to use the EFT to derive a more limited number of parameters. Individual spreadsheets are generally self-contained and all automatically populated data, placed in cells with a light background, can be overwritten. It is suggested that the minimum requirements listed in Table 2 are met, and to ensure that all datapoints and parameters used in the calculations are available. If some values are taken from the literature, consistency with the dataset should be checked. Individual sheets may be copied and used separately for convenience.

Intermediate and Engineered assimilatory pathways

Concerns for global warming and increasing human population have directed considerable effort towards improving plant photosynthetic efficiency. The possible improvement strategies (Singh *et al.*, 2014, Zhu *et al.*, 2010) together with the most relevant indicators for detecting variability through the EFT can be summarised as follows:

Carbon assimilation

Rubisco CO_2 fixation capacity and CO_2/O_2 specificity (Carmo-Silva *et al.*, 2014) are targets for improvement in a C_3 plant, and the EFT can be used to mechanistically derive Rubisco

specificity $S_{C/O}$ (or Γ^*), and Rubisco affinity $K_C(1+O/K_O)$ in sheets 11 and 13. These C_3 mechanistic models cannot be used when the goal is to modify the CO_2/O_2 ratio at the carboxylation sites by introducing an active biochemical or biophysical carbon concentrating mechanism (CCM), and any associated anatomical modifications (Kajala *et al.*, 2011, Maurino & Weber, 2013, Meyer & Griffiths, 2013). In fact, assessing the efficiency of a CCM involves screening populations of C_3-C_4 hybrids, C_2-cycle variants, C_3 plants (or algae) displaying intermediate C_4 traits, or C_4 mutants lacking a fully functional CCM. In this case, data analysis cannot assume 'C_3ness' and sheets 11, 12 and 13, cannot be used. However, empirical modelling and *J* values are valid (sheets 1 – 10), as the NADPH demand is the same for all pathways of assimilation. *CE* will promptly detect different relative affinities for CO_2 or activities of Rubisco and/or PEPC. C_{i50} is often used as an apparent *in vivo* indicator of affinity for CO_2 analogous to $K_{1/2}$ [for instance, to follow CCM induction in aquatic photosynthesis (Mitchell *et al.*, 2014)]. CO_2/O_2 specificity correlates with C_i^*, which, because it is independent of the dynamics of R_{LIGHT} (Bellasio & Griffiths, 2014a, Gandin *et al.*, 2014), is more appropriate to follow than Γ. V_O/V_C shows the final effect of the CCM on photorespiratory suppression (Bellasio *et al.*, 2014). If V_O/V_C calculated with the EFT is to be compared to V_O/V_C calculated with a conventional C_4 or C_3-C_4 model, note that limiting NADPH is assumed via the EFT, whilst limiting ATP is often assumed for C_4 and C_3-C_4 photosynthesis (Bellasio & Griffiths, 2014c, von Caemmerer, 2000, Yin *et al.*, 2011b).

CO₂ recapture

The reciprocal position of mitochondria and chloroplasts have been targeted to increase photorespiration recapture (Busch *et al.*, 2013). The quantities of interest in this case are V_O/V_C and C_i^* for the reasons highlighted above.

Photochemistry

Optimisation strategies include reducing the fraction of light harvested by PSII in the upper layers of chloroplasts or leaves of a canopy (Tholen *et al.*, 2012a), and can be investigated using the EFT through *s* or $\alpha\beta$, the overall fraction of light harvested by PSII. Stress events affecting the electron transport chain can be followed through the quantities J_{SAT} and $PPFD_{50}$, which describe the *PPFD* dependence of *J*. Permanent PSII inhibition will influence $Y(II)_{LL}$. $Y(J)_{LL}$ and $Y(CO_2)_{LL}$ aggregate the effect of *s* or $\alpha\beta$ and $Y(II)_{LL}$.

CO₂ diffusion

Optimisation strategies include facilitating CO_2 penetration in the chloroplast to increase C_C/C_i. The most significant quantity to follow is g_M, the derivation of which using the EFT is valid only for C_3 plants.

Shade tolerance

Optimisation strategies may act on plant acclimation plasticity or modify permanent traits (adaptation) with the final goal of improving efficiency of the considerable fraction of crop photosynthesis carried out in the shade (Bellasio & Griffiths, 2014a, Bellasio & Griffiths, 2014b, Craine & Reich, 2005, Sage, 2013). The most significant quantities to follow are *LCP* and R_{LIGHT}.

Induction of CAM metabolism

Some of the EFT features have proved useful for studying CAM metabolism (Jamie Males, personal communication). Sheets 1-13 are fully functional during phase IV (late afternoon CO_2 fixation) when CAM plants are functioning as C_3. Under these conditions *αβ* or *s* could be calibrated and then used to resolve C_3 and CAM contributions to CO_2 fixation in other CAM phases, for instance by inputting *Y(II)* and a set of simulated C_i values (Owen & Griffiths, 2013) to Eqn 19 (Sheet 12).

Worked example applying the EFT to primary data from *Nicotiana tabacum* L.

Tobacco plants were grown in controlled environment growth rooms (BDR 16, Conviron Ltd, Winnipeg, Canada) set at 14h day length, *PPFD* = 350 μmol m^{-2} s^{-1}, temperature of 27 °C / 18 °C (day / night), 70 % relative humidity. Plants were manually watered daily, with particular care to avoid overwatering. Four photosynthetic response curves (an *A/C_i* and a light-curve under ambient and low O_2) were measured on *n*=4 plants with an infra-red gas analyser (IRGA, LI6400XT, LI-COR, USA), fitted with a 6400-40 leaf chamber fluorometer, details are reported in Supporting Information Note 2. Primary data were corrected for CO_2 diffusion through the gaskets (Boesgaard *et al.*, 2013) as:

$$A = Photo + \frac{0.46\,(400 - C_a)}{100\;Area} \qquad\qquad 21$$

Where *Photo* is the uncorrected assimilation as calculated by the LI-COR software, 400 is the external CO_2 concentration, C_a is the CO_2 concentration in the cuvette (CO2S in the LI-COR notation) and *Area* is the leaf area (2 cm^2 in this example). C_i was recalculated using the LI-COR equations inputting *A* calculated with Eqn 21. Diffusion-corrected data are shown in Figure 1 (individual values are reported in Supporting Information). Under high *PPFD*, *A* was lower under ambient O_2 (closed symbols) than under low O_2 (open symbols) because of the operating PCO cycle. Under low O_2, *Y(II)* was slightly lower (dotted line) reflecting lower reducing power demand

(Figure 1A). Under low C_i, A was higher under low O_2 (open symbols) than under ambient O_2 (closed symbols) because of O_2 competitive inhibition of Rubisco. Under high C_i, A was unaffected by CO_2 concentration and slightly higher under ambient O_2, suggesting that assimilation was TPU-limited. Under these conditions $Y(II)$ was slightly lower under low O_2 (dotted line) for the lower reducing power demand (Figure 1B), showing a tight feedback on $Y(II)$ even under TPU limitation. Data were analysed using the 13-step approach of the EFT, summarised below. Rather than providing a recipe for data analysis we aimed at showing some of the numerous available alternatives, the choice of which may vary depending on the experimental requirements.

1. Thresholds used to assign datapoints to limited regions of the response curves (entered as 1, 2) or regions of saturating inputs (3) were, for light-curves: '1' $PPFD \leq 100$ µmol m^{-2} s^{-1}; '2' $PPFD$ =150 and $PPFD = 200$ µmol m^{-2} s^{-1}; '3' $PPFD \geq 500$ µmol m^{-2} s^{-1}. For A/C_i curves: '1' $C_i \leq 100$ µmol mol^{-1}; '2' $100 < C_i < 260$ µmol mol^{-1}; '3' $C_i \geq 260$ µmol mol^{-1}

2. R_{LIGHT} was derived under ambient and low O_2 using linear regressions (Eqn 1), values did not substantially differ from R_{DARK} which may be added to the regressions to increase constraint. R_{LIGHT} derived with the BF method (under high $PPFD$) was slightly lower than R_{DARK}, but note that the BF method is subject the effect of CO_2 diffusion (see Supporting Information Note 1).

3. $Y(II)_{LL}$ did not vary between plants. For comparison, we present the results of linear, exponential and quadratic regressions. The quadratic regression yielded slightly higher $Y(II)_{LL}$ especially under low O_2 with a better fit (c. 1.000 vs c. 0.999), and may be considered in further studies, however in the following steps for consistency with Yin et $al.$ (2014) we used the linear $Y(II)_{LL}$.

4. GA was calculated under ambient and low O_2 using the values of R_{LIGHT} derived in Step 2. The $PPFD$ dependence of GA was modelled and GA_{SAT}, $PPFD_{50}$ and $Y(CO_2)_{LL}$ were derived by non-linear curve-fitting. The LCP was higher under ambient O_2 reflecting the additional light requirements for operating the PCO cycle. GA_{SAT} was higher under low O_2 because of the additional ATP and NADPH availability for CO_2 assimilation. $Y(CO_2)_{LL}$ was higher under low O_2 reflecting the higher conversion efficiency of light into fixed CO_2, the alternative liner fitting of (Yin et $al.$, 2014) yielded similar $Y(CO_2)_{LL}$; a lower $PPFD_{50}$ under low O_2 reflected a steeper light-curve.

5. The C_i dependence of A was modelled under ambient and low O_2 and CE, A_{SAT}, C_{i50} and Γ were derived by non-linear curve-fitting. Residuals were log-transformed to correct for proportionality between residuals and A, thus providing a better fit in the low C_i region of the modelled curve. CE was higher under low O_2, reflecting the slope of the A/C_i curve. C_{i50} was lower under low O_2 reflecting a faster saturation. C_i* was calculated from the fitted curve using R_{LIGHT} derived in Step 2 under ambient or low O_2 respectively. L_S was assessed from the fitted curve. TPU was calculated from the last datapoint of A/C_i curves under ambient and low O_2.

6a. The Yin calibration was performed with standard settings.

6b. The Valentini calibration was performed using R_{LIGHT} estimated in Step 2 and pooling all datapoints measured under low O_2. The parameter, b, which is responsible for differences between the Valentini and Yin J values at high $PPFD$ (see 9), was substantially different from 0.

7. $Y(J)_{LL}$ did not vary between O_2 levels or the calibration approach, in good agreement with theoretical considerations (Farquhar *et al.*, 1980), however, it did differ from the generally assumed value of 0.361 [0.85×½×0.85 (von Caemmerer, 2000)], confirming the importance calibrating each leaf.

8. J was calculated with Eqn 9, 10 and 11 (individual values not shown in Table 3).

9. The $PPFD$ response of J was modelled to derive J_{SAT}, θ and $PPFD_{50}$. The three approaches gave different results: the Yin calibration resulted in the highest J_{SAT} and $PPFD_{50}$ while the Bellasio and Valentini calibration yielded lower values, as theoretically expected (see Step 8 above).

10. All quantities associated with Rubisco rate of carboxylation and oxygenation were calculated for each datapoint using three approaches to calculating J (individual values not shown in Table 3).

11. $S_{C/O}$ was derived in Sheet 11 with the (suggested) non-linear variant of the method of Yin described above, using the fitted value for R_{LIGHT} and the non-linear estimates of CE derived under ambient and low O_2 in Sheet 5. Residuals were log-transformed to correct for proportionality between residuals and A. $S_{C/O}$ was averaged, the average value was in good agreement with published values (Ethier & Livingston, 2004, von Caemmerer, 2000) and was used in steps 12 and 13. For comparison $S_{C/O}$ was derived with the original method of Yin, using linear estimates for CE (shown in additional features of Sheet 11). Because, under ambient O_2, the linear fit gave slightly lower CE, $S_{C/O}$ was slightly overestimated (Table 3). For additional comparison, $S_{C/O}$ was derived as $S_{C/O} = \frac{0.5O}{c_i^*}$ (Laisk), which tends to overestimate $S_{C/O}$ for the reasons previously described.

12. g_M was determined by fitting data pooled from the light limited region of the light and A/C_i curves, using R_{LIGHT} derived under ambient O_2 in Sheet 2, J calculated with the three approaches described in Step 8, and the average value of $S_{C/O}$ found in 11. Overall g_M values are in line with literature reports (Flexas *et al.*, 2012), however, the calibration of Yin resulted in a lower g_M and R^2 likely for the theoretical reasons highlighted in Step 8.

13. V_{CMAX} and $K_C(1+O/K_O)$ were estimated by fitting Eqn 20 to ambient O_2 A/C_i curves, using R_{LIGHT}, and Γ derived in Step 2 and 5a respectively, and g_M derived in Step 12 using three different calculations of J. The higher g_M values obtained with the Bellasio calibration yielded $K_C(1+O/K_O)$ estimates similar to those of Ethier and Livingston (2004), whereas the lower g_M values obtained with the Yin calibration prevented to fit $K_C(1+O/K_O)$. In addition, V_{CMAX} and $K_C(1+O/K_O)$ were estimated from low O_2 A/C_i curves, with R_{LIGHT} and Γ derived under low O_2 in Step 2 and 5b respectively. Under low O_2 $K_C(1+O/K_O)$ values differed from the expected (c. 350 µmol mol^{-1}), could not be fitted with the Yin estimates for g_M and reflected on V_{CMAX} values. When the values

for $K_C(1+O/K_O)$ appear not to be physiologically realistic (in this example under low O_2 and under ambient O_2 when g_M is lower than 0.3) it is probably appropriate to constrain $K_C(1+O/K_O)$ with a literature value (see instructions in Sheet 13). As an additional feature, V_{CMAX} was fitted concurrently to ambient and low O_2 A/C_i curves after constraining $K_C(1+O/K_O)$ with values from Ethier and Livingston (2004). This simple and reliable procedure (C.V. was as low as 9 %) may be highly valuable for future studies.

Conclusion

Using combined fluorescence-A/C_i and fluorescence-light-response curves, measured under ambient and low O_2, the Excel-based fitting tool (EFT) can be used to derive a comprehensive suite of physiological parameters. The EFT uses step-by-step logic to derive parameters, which are then used in the following steps, thus avoiding many of the uncertainties associated with the conventional A/C_i fitting and concurrent multimodel applications. All steps are implemented in a freely downloadable Excel workbook that is easily modified by the user. The derived parameters summarise the physiological traits of the plant(s) measured and can be used to compare different plants or to parameterise predictive models. Overall, the EFT integrates the latest developments in the theory of gas exchange, fluorescence and mesophyll limitations, and provides advanced analytical outputs. This allows both specialist and non-specialist researchers to apply EFT outputs when screening plant populations for phenotypic or genotypic impacts upon photosynthetic operating efficiencies, or the complete parameterisation of modern predictive models.
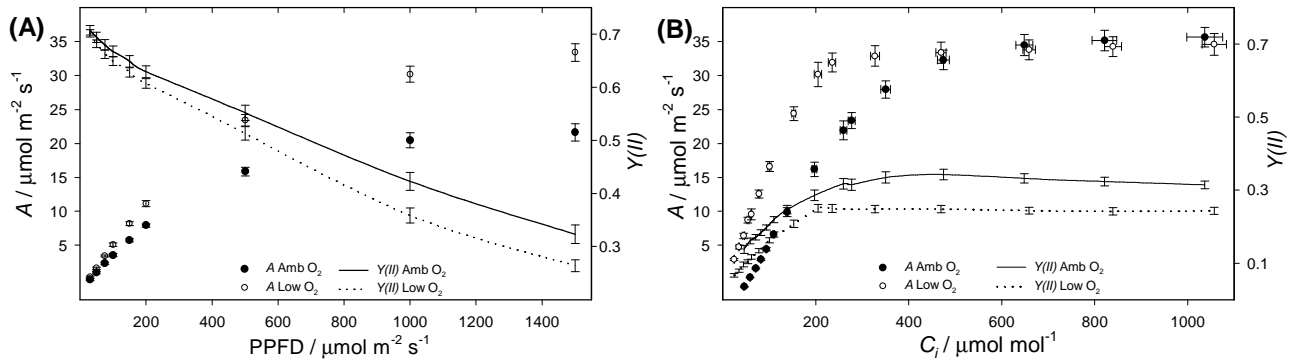
References

Baker N.R. (2008) Chlorophyll fluorescence: A probe of photosynthesis in vivo. *Annual Review of Plant Biology*, **59**, 89-113.

Bellasio C., Burgess S.J., Griffiths H. & Hibberd J.M. (2014) A high throughput gas exchange screen for determining rates of photorespiration or regulation of C4 activity. *Journal of Experimental Botany*, **65**, 3769-3779.

Bellasio C. & Griffiths H. (2014a) Acclimation of C4 metabolism to low light in mature maize leaves could limit energetic losses during progressive shading in a crop canopy. *Journal of Experimental Botany*, **65**, 3725-3736.

Bellasio C. & Griffiths H. (2014b) Acclimation to Low Light by C4 maize: Implications for Bundle Sheath Leakiness. *Plant Cell and Environment*, **37**, 1046-1058.

Bellasio C. & Griffiths H. (2014c) The operation of two decarboxylases (NADPME and PEPCK), transamination and partitioning of C4 metabolic processes between mesophyll and bundle sheath cells allows light capture to be balanced for the maize C4 pathway. *Plant Physiology*, **164**, 466-480.

Bernacchi C.J., Bagley J.E., Serbin S.P., Ruiz-Vera U.M., Rosenthal D.M. & Vanloocke A. (2013) Modelling C3 photosynthesis from the chloroplast to the ecosystem. *Plant Cell and Environment*, **36**, 1641-1657.

Bernacchi C.J., Pimentel C. & Long S.P. (2003) In vivo temperature response functions of parameters required to model RuBP-limited photosynthesis. *Plant, Cell & Environment*, **26**, 1419-1430.

Bernacchi C.J., Portis A.R., Nakano H., von Caemmerer S. & Long S.P. (2002) Temperature Response of Mesophyll Conductance. Implications for the Determination of Rubisco Enzyme Kinetics and for Limitations to Photosynthesis in Vivo. *Plant Physiology*, **130**, 1992-1998.

Bernacchi C.J., Singsaas E.L., Pimentel C., Portis Jr A.R. & Long S.P. (2001) Improved temperature response functions for models of Rubisco-limited photosynthesis. *Plant, Cell & Environment*, **24**, 253-259.

Boesgaard K.S., Mikkelsen T.N., Ro-Poulsen H. & Ibrom A. (2013) Reduction of molecular gas diffusion through gaskets in leaf gas exchange cuvettes by leaf-mediated pores. *Plant, Cell & Environment*, **36**, 1352-1362.

Boote K.J., Jones J.W., White J.W., Asseng S. & Lizaso J.I. (2013) Putting mechanisms into crop production models. *Plant Cell and Environment*, **36**, 1658-1672.

Brooks A. & Farquhar G.D. (1985) Effect of temperature on the CO2/O2 specificity of ribulose-1,5-bisphosphate carboxylase/oxygenase and the rate of respiration in the light. *Planta*, **165**, 397-406.

Buckley T.N. & Adams M.A. (2011) An analytical model of non-photorespiratory CO2 release in the light and dark in leaves of C3 species based on stoichiometric flux balance. *Plant, Cell & Environment*, **34**, 89-112.

Buckley T.N. & Diaz-Espejo A. (2014) Reporting estimates of maximum potential electron transport rate. *New Phytologist*, **205**, 14–17.

Buckley T.N. & Warren C.R. (2014) The role of mesophyll conductance in the economics of nitrogen and water use in photosynthesis. *Photosynthesis Research*, **119**, 77-88.

Busch F.A., Sage T.L., Cousins A.B. & Sage R.F. (2013) C3 plants enhance rates of photosynthesis by reassimilating photorespired and respired CO2. *Plant, Cell & Environment*, **36**, 200-212.

Carmo-Silva E., Scales J.C., Madgwick P.J. & Parry M.A.J. (2014) Optimizing Rubisco and its regulation for greater resource use efficiency. *Plant, Cell & Environment*, **205**, 14-17.

Cernusak L.A., Ubierna N., Winter K., Holtum J.A.M., Marshall J.D. & Farquhar G.D. (2013) Environmental and physiological determinants of carbon isotope discrimination in terrestrial plants. *New Phytologist*, **200**, 950-965.

Cousins A.B., Ghannoum O., Von Caemmerer S. & Badger M.R. (2010) Simultaneous determination of Rubisco carboxylase and oxygenase kinetic parameters in Triticum aestivum and Zea mays using membrane inlet mass spectrometry. *Plant, Cell & Environment*, **33**, 444-452.

Craine J.M. & Reich P.B. (2005) Leaf-level light compensation points in shade-tolerant woody seedlings. *New Phytologist*, **166**, 710-713.

Delgado E., Medrano H., Keys A.J. & Parry M.A.J. (1995) Species variation in Rubisco specificity factor. *Journal of Experimental Botany*, **46**, 1775-1777.

Drake B.G., GonzalezMeler M.A. & Long S.P. (1997) More efficient plants: A consequence of rising atmospheric CO2? *Annual Review of Plant Physiology and Plant Molecular Biology*, **48**, 609-639.

Eckardt N.A. (2005) Photorespiration Revisited. *The Plant Cell*, **17**, 2139-2141.

Ethier G.J. & Livingston N.J. (2004) On the need to incorporate sensitivity to CO2 transfer conductance into the Farquhar-von Caemmerer-Berry leaf photosynthesis model. *Plant Cell and Environment*, **27**, 137-153.

Evans J.R. (1987) The Dependence of Quantum Yield on Wavelength and Growth Irradiance. *Australian Journal of Plant Physiology*, **14**, 69-79.

Evans J.R. (2009) Potential Errors in Electron Transport Rates Calculated from Chlorophyll Fluorescence as Revealed by a Multilayer Leaf Model. *Plant and Cell Physiology*, **50**, 698-706.

Evans J.R. (2013) Gas exchange measurements of photosynthetic response curves. PrometheusWiki.

Evans J.R., Kaldenhoff R., Genty B. & Terashima I. (2009) Resistances along the CO2 diffusion pathway inside leaves. *Journal of Experimental Botany*, **60**, 2235-2248.

Evans J.R. & Loreto F. (2000) Acquisition and diffusion of CO2 in higher plant leaves. In: *Photosynthesis: Physiology and metabolism*, pp. 321-351. Kluwer Academic Publishers.

Evans J.R. & von Caemmerer S. (1996) Carbon dioxide diffusion inside leaves. *Plant Physiology*, **110**, 339-346.

Farquhar G.D. & Sharkey T.D. (1982) Stomatal Conductance and Photosynthesis. *Annual Review of Plant Physiology and Plant Molecular Biology*, **33**, 317-345.

Farquhar G.D., von Caemmerer S. & Berry J.A. (1980) A biochemical-model of photosynthetic CO2 assimilation in leaves of C3 species. *Planta*, **149**, 78-90.

Farquhar G.D. & Wong S.C. (1984) An Empirical-Model of Stomatal Conductance. *Australian Journal of Plant Physiology*, **11**, 191-209.

Flexas J., Barbour M.M., Brendel O., Cabrera H.M., Carriqui M., Diaz-Espejo A., Douthe C., Dreyerc E., Ferrio J.P., Gago J., Galle A., Galmes J., Kodama N., Medrano H., Niinemets U., Peguero-Pina J.J., Poua A., Ribas-Carbo M., Tomas M., Tosens T. & Warren C.R. (2012) Mesophyll diffusion conductance to CO2: An unappreciated central player in photosynthesis (vol 193, pg 70, 2012). *Plant Science*, **196**, 31-31.

Flexas J., Diaz-Espejo A., GalmÉS J., Kaldenhoff R., Medrano H. & Ribas-Carbo M. (2007) Rapid variations of mesophyll conductance in response to changes in CO2 concentration around leaves. *Plant, Cell & Environment*, **30**, 1284-1298.

Flexas J., Loreto F., Niinemets U. & Sharkey T. (2009) Special Issue: Mesophyll conductance to CO2: mechanisms, modelling, and ecological implications Preface. *Journal of Experimental Botany*, **60**, 2215-2216.

Flexas J., Ribas-Carbó M., Diaz-Espejo A., GalmÉS J. & Medrano H. (2008) Mesophyll conductance to CO2: current knowledge and future prospects. *Plant, Cell & Environment*, **31**, 602-621.

Flexas J., Ribas-Carbó M., Hanson D.T., Bota J., Otto B., Cifre J., McDowell N., Medrano H. & Kaldenhoff R. (2006) Tobacco aquaporin NtAQP1 is involved in mesophyll conductance to CO2 in vivo. *The Plant Journal*, **48**, 427-439.

Galmés J., Flexas J., Keys A.J., Cifre J., Mitchell R.A.C., Madgwick P.J., Haslam R.P., Medrano H. & Parry M.A.J. (2005) Rubisco specificity factor tends to be larger in plant species from drier habitats and in species with persistent leaves. *Plant, Cell & Environment*, **28**, 571-579.

Galmés J., Medrano H. & Flexas J. (2006) Acclimation of Rubisco specificity factor to drought in tobacco: discrepancies between in vitro and in vivo estimations. *Journal of Experimental Botany*, **57**, 3659-3667.

Gandin A., Koteyeva N.K., Voznesenskaya E.V., Edwards G.E. & Cousins A.B. (2014) The acclimation of photosynthesis and respiration to temperature in the C3–C4 intermediate Salsola divaricata: induction of high respiratory CO2 release under low temperature. *Plant, Cell & Environment*, **37**, 2601–2612.

Genty B., Briantais J.M. & Baker N.R. (1989) The relationship between the quantum yield of photosynthetic electron-transport and quenching of chlorophyll fluorescence. *Biochimica Et Biophysica Acta*, **990**, 87-92.

Gilbert M.E., Pou A., Zwieniecki M.A. & Holbrook N.M. (2012) On measuring the response of mesophyll conductance to carbon dioxide with the variable J method. *Journal of Experimental Botany*, **63**, 413-425.

Gu L., Pallardy S.G., Tu K., Law B.E. & Wullschleger S.D. (2010) Reliable estimation of biochemical parameters from C3 leaf photosynthesis–intercellular carbon dioxide response curves. *Plant, Cell & Environment*, **33**, 1852-1874.

Gu L. & Sun Y. (2014) Artefactual responses of mesophyll conductance to CO_2 and irradiance estimated with the variable J and online isotope discrimination methods. *Plant, Cell & Environment*, **37**, 1231-1249.

Harbinson J. (2013) Improving the accuracy of chlorophyll fluorescence measurements. *Plant, Cell & Environment*, **36**, 1751-1754.

Harley P. & Sharkey T. (1991) An improved model of C3 photosynthesis at high CO_2: Reversed O_2 sensitivity explained by lack of glycerate reentry into the chloroplast. *Photosynthesis Research*, **27**, 169-178.

Harley P.C., Loreto F., Di Marco G. & Sharkey T.D. (1992) Theoretical Considerations when Estimating the Mesophyll Conductance to CO_2 Flux by Analysis of the Response of Photosynthesis to CO_2. *Plant Physiology*, **98**, 1429-1436.

Heckwolf M., Pater D., Hanson D.T. & Kaldenhoff R. (2011) The Arabidopsis thaliana aquaporin AtPIP1;2 is a physiologically relevant CO_2 transport facilitator. *Plant Journal*, **67**, 795-804.

June T., Evans J.R. & Farquhar G.D. (2004) A simple new equation for the reversible temperature dependence of photosynthetic electron transport: a study on soybean leaf. *Functional Plant Biology*, **31**, 275-283.

Kajala K., Covshoff S., Karki S., Woodfield H., Tolley B.J., Dionora M.J.A., Mogul R.T., Mabilangan A.E., Danila F.R., Hibberd J.M. & Quick W.P. (2011) Strategies for engineering a two-celled C4 photosynthetic pathway into rice. *Journal of Experimental Botany*, **62**, 3001-3010.

Keurentjes J.J.B., Molenaar J. & Zwaan B.J. (2013) Predictive modelling of complex agronomic and biological systems. *Plant Cell and Environment*, **36**, 1700-1710.

Kok B. (1948) A critical consideration of the quantum yield of Chlorella photosynthesis. *Enzymologia*, **13**, 625-631.

Kromdijk J., Griffiths H. & Schepers H.E. (2010) Can the progressive increase of C4 bundle sheath leakiness at low PFD be explained by incomplete suppression of photorespiration? *Plant Cell and Environment*, **33**, 1935-1948.

Laisk A. (1977) Kinetics of photosynthesis and photorespiration in C3 plants. *Nauka Moscow*.

Laisk A., Oja V., Rasulov B., Ramma H., Eichelmann H., Kasparova I., Pettai H., Padu E. & Vapaavuori E. (2002) A computer-operated routine of gas exchange and optical measurements to diagnose photosynthetic apparatus in leaves. *Plant Cell and Environment*, **25**, 923-943.

Long S.P. & Bernacchi C.J. (2003) Gas exchange measurements, what can they tell us about the underlying limitations to photosynthesis? Procedures and sources of error. *Journal of Experimental Botany*, **54**, 2393-2401.

Long S.P., Farage P.K. & Garcia R.L. (1996) Measurement of leaf and canopy photosynthetic CO_2 exchange in the field. *Journal of Experimental Botany*, **47**, 1629-1642.

Loriaux S.D., Avenson T.J., Welles J.M., McDermitt D.K., Eckles R.D., Riensche B. & Genty B. (2013) Closing in on maximum yield of chlorophyll fluorescence using a single multiphase flash of sub-saturating intensity. *Plant, Cell & Environment*, **36**, 1755-1770.

Martins S.C.V., Galmés J., Molins A. & DaMatta F.M. (2013) Improving the estimation of mesophyll conductance to CO_2: on the role of electron transport rate correction and respiration. *Journal of Experimental Botany*, **64**, 3285-3298.

Maurino V.G. & Weber A.P.M. (2013) Engineering photosynthesis in plants and synthetic microorganisms. *Journal of Experimental Botany*, **64**, 743-751.

Maxwell K. & Johnson G.N. (2000) Chlorophyll fluorescence - a practical guide. *Journal of Experimental Botany*, **51**, 659-668.

Melton J.R., Wania R., Hodson E.L., Poulter B., Ringeval B., Spahni R., Bohn T., Avis C.A., Beerling D.J., Chen G., Eliseev A.V., Denisov S.N., Hopcroft P.O., Lettenmaier D.P., Riley W.J., Singarayer J.S., Subin Z.M., Tian H., Zürcher S., Brovkin V., van Bodegom P.M., Kleinen T., Yu Z.C. & Kaplan J.O. (2013) Present state of global wetland extent and wetland methane modelling: conclusions from a model inter-comparison project (WETCHIMP). *Biogeosciences*, **10**, 753-788.

Meyer M. & Griffiths H. (2013) Origins and diversity of eukaryotic CO_2-concentrating mechanisms: lessons for the future. *Journal of Experimental Botany*, **64**, 769-786.

Mitchell M.C., Griffiths H. & Meyer M.T. (2014) Dynamics of carbon concentrating mechanism induction and protein re-localisation during the dark to light transition in synchronised Chlamydomonas. *Plant Physiology*.

Murchie E.H. & Lawson T. (2013) Chlorophyll fluorescence analysis: a guide to good practice and understanding some new applications. *Journal of Experimental Botany*, **64**, 3983-3998.

Niinemets U., Diaz-Espejo A., Flexas J., Galmes J. & Warren C.R. (2009a) Importance of mesophyll diffusion conductance in estimation of plant photosynthesis in the field. *Journal of Experimental Botany*, **60**, 2271-2282.

Niinemets U., Diaz-Espejo A., Flexas J., Galmes J. & Warren C.R. (2009b) Role of mesophyll diffusion conductance in constraining potential photosynthetic productivity in the field. *Journal of Experimental Botany*, **60**, 2249-2270.

Owen N.A. & Griffiths H. (2013) A system dynamics model integrating physiology and biochemical regulation predicts extent of crassulacean acid metabolism (CAM) phases. *New Phytologist*, **200**, 1116-1131.

Papageorgiou G.C. (2004) *Chlorophyll a fluorescence: a signature of photosynthesis* (vol. 19). Springer.

Parkhurst D.F. & Mott K.A. (1990) Intercellular Diffusion Limits to CO_2 Uptake in Leaves. *Plant Physiology*, **94**, 1024-1032.

Parry M.A.J., Keys A.J. & Gutteridge S. (1989) Variation in the Specificity Factor of C3 Higher Plant Rubiscos Determined by the Total Consumption of Ribulose-P2. *Journal of Experimental Botany*, **40**, 317-320.

Pons T.L., Flexas J., von Caemmerer S., Evans J.R., Genty B., Ribas-Carbo M. & Brugnoli E. (2009) Estimating mesophyll conductance to CO_2: methodology, potential errors, and recommendations. *Journal of Experimental Botany*, **60**, 2217-2234.

Prioul J.L. & Chartier P. (1977) Partitioning of Transfer and Carboxylation Components of Intracellular Resistance to Photosynthetic CO_2 Fixation: A Critical Analysis of the Methods Used. *Annals of Botany*, **41**, 789-800.

Sage R.F. (2013) Stopping the leaks: New insights into C4 photosynthesis at low light. *Plant, Cell & Environment*, **doi/10.1111/pce.12246**.

Scafaro A.P., Von Caemmerer S., Evans J.R. & Atwell B.J. (2011) Temperature response of mesophyll conductance in cultivated and wild Oryza species with contrasting mesophyll cell wall thickness. *Plant, Cell & Environment*, **34**, 1999-2008.

Schansker G., Toth S.Z., Holzwarth A.R. & Garab G. (2014) Chlorophyll a fluorescence: beyond the limits of the Q(A) model. *Photosynthesis Research*, **120**, 43-58.

Sharkey T.D., Bernacchi C.J., Farquhar G.D. & Singsaas E.L. (2007) Fitting photosynthetic carbon dioxide response curves for C3 leaves. *Plant Cell and Environment*, **30**, 1035-1040.

Singh J., Pandey P., James D., Chandrasekhar K., Achary V.M.M., Kaul T., Tripathy B.C. & Reddy M.K. (2014) Enhancing C3 photosynthesis: an outlook on feasible interventions for crop improvement. *Plant Biotechnology Journal*, **12**, 1217-1230.

Stirbet A. & Govindjee (2011) On the relation between the Kautsky effect (chlorophyll a fluorescence induction) and Photosystem II: Basics and applications of the OJIP fluorescence transient. *Journal of Photochemistry and Photobiology B: Biology*, **104**, 236-257.

Sun J., Feng Z., Leakey A.D.B., Zhu X., Bernacchi C.J. & Ort D.R. (2014a) Inconsistency of mesophyll conductance estimate causes the inconsistency for the estimates of maximum rate of Rubisco carboxylation among the linear, rectangular and non-rectangular hyperbola biochemical models of leaf photosynthesis—A case study of CO_2 enrichment and leaf aging effects in soybean. *Plant Science*, **226**, 49-60.

Sun Y., Gu L.H., Dickinson R.E., Norby R.J., Pallardy S.G. & Hoffman F.M. (2014b) Impact of mesophyll diffusion on estimated global land CO_2 fertilization. *Proceedings of the National Academy of Sciences of the United States of America*, **111**, 15774-15779.

Tazoe Y., Von Caemmerer S., Estavillo G.M. & Evans J.R. (2011) Using tunable diode laser spectroscopy to measure carbon isotope discrimination and mesophyll conductance to CO_2 diffusion dynamically at different CO_2 concentrations. *Plant, Cell & Environment*, **34**, 580-591.

Tcherkez G., Bligny R., Gout E., Mahé A., Hodges M. & Cornic G. (2008) Respiratory metabolism of illuminated leaves depends on CO2 and O2 conditions. *Proceedings of the National Academy of Sciences*, **105**, 797-802.

Terashima I., Fujita T., Inoue T., Chow W.S. & Oguchi R. (2009) Green Light Drives Leaf Photosynthesis More Efficiently than Red Light in Strong White Light: Revisiting the Enigmatic Question of Why Leaves are Green. *Plant and Cell Physiology*, **50**, 684-697.

Terashima I., Hanba Y.T., Tholen D. & Niinemets U. (2011) Leaf Functional Anatomy in Relation to Photosynthesis. *Plant Physiology*, **155**, 108-116.

Thakur A. (1991) Model: Mechanistic vs Empirical. In: *New Trends in Pharmacokinetics* (eds A. Rescigno & A. Thakur), pp. 41-51. Springer US.

Tholen D., Boom C. & Zhu X.-G. (2012a) Opinion: Prospects for improving photosynthesis by altering leaf anatomy. *Plant Science*, **197**, 92-101.

Tholen D., ÉThier G. & Genty B. (2014) Mesophyll conductance with a twist. *Plant, Cell & Environment*, **37**, 2456–2458.

Tholen D., Ethier G., Genty B., Pepin S. & Zhu X.G. (2012b) Variable mesophyll conductance revisited: theoretical background and experimental implications. *Plant Cell and Environment*, **35**, 2087-2103.

Tholen D. & Zhu X.G. (2011) The Mechanistic Basis of Internal Conductance: A Theoretical Analysis of Mesophyll Cell Photosynthesis and CO2 Diffusion. *Plant Physiology*, **156**, 90-105.

Timm H., Stegemann J. & Küppers M. (2002) Photosynthetic induction strongly affects the light compensation point of net photosynthesis and coincidentally the apparent quantum yield. *Trees*, **16**, 47-62.

Valentini R., Epron D., De Angelis P., Matteucci G. & Dreyer E. (1995) In situ estimation of net CO2 assimilation, photosynthetic electron flow and photorespiration in Turkey oak (Q. cerris L) leaves: diurnal cycles under different levels of water supply. *Plant, Cell & Environment*, **18**, 631-640.

von Caemmerer S. (2000) *Biochemical models of leaf Photosynthesis*. CSIRO Publishing, Collingwood.

von Caemmerer S. (2013) Steady-state models of photosynthesis. *Plant, Cell & Environment*, **36**, 1617-1630.

von Caemmerer S. & Evans J.R. (1991) Determination of the Average Partial-Pressure of CO2 in Chloroplasts from Leaves of Several C3 Plants. *Australian Journal of Plant Physiology*, **18**, 287-305.

von Caemmerer S. & Farquhar G.D. (1981) Some Relationships between the Biochemistry of Photosynthesis and the Gas-Exchange of Leaves. *Planta*, **153**, 376-387.

von Caemmerer S., Ghannoum O., Pengelly J.J.L. & Cousins A.B. (2014) Carbon isotope discrimination as a tool to explore C4 photosynthesis. *Journal of Experimental Botany*.

Walters M.B. & Reich P.B. (1996) Are Shade Tolerance, Survival, and Growth Linked? Low Light and Nitrogen Effects on Hardwood Seedlings. *Ecology*, **77**, 841-853.

Warren C. (2006) Estimating the internal conductance to CO2 movement. *Functional Plant Biology*, **33**, 431-442.

Woodward F.I. & Lomas M.R. (2004) Vegetation dynamics - simulating responses to climatic change. *Biological Reviews*, **79**, 643-670.

Yamori W. & von Caemmerer S. (2009) Effect of Rubisco Activase Deficiency on the Temperature Response of CO2 Assimilation Rate and Rubisco Activation State: Insights from Transgenic Tobacco with Reduced Amounts of Rubisco Activase. *Plant Physiology*, **151**, 2073-2082.

Yin X., Belay D., van der Putten P.L. & Struik P. (2014) Accounting for the decrease of photosystem photochemical efficiency with increasing irradiance to estimate quantum yield of leaf photosynthesis. *Photosynthesis Research*, 1-13.

Yin X. & Struik P.C. (2009a) C3 and C4 photosynthesis models: An overview from the perspective of crop modelling. *Njas-Wageningen Journal of Life Sciences*, **57**, 27-38.

Yin X. & Struik P.C. (2010) Modelling the crop: from system dynamics to systems biology. *Journal of Experimental Botany*, **61**, 2171-2183.

Yin X., Struik P.C., Romero P., Harbinson J., Evers J.B., Van Der Putten P.E.L. & Vos J.A.N. (2009) Using combined measurements of gas exchange and chlorophyll fluorescence to estimate parameters of a biochemical C3 photosynthesis model: a critical appraisal and a new integrated approach applied to leaves in a wheat (Triticum aestivum) canopy. *Plant, Cell & Environment*, **32**, 448-464.

Yin X., Sun Z., Struik P.C. & Gu J. (2011a) Evaluating a new method to estimate the rate of leaf respiration in the light by analysis of combined gas exchange and chlorophyll fluorescence measurements. *Journal of Experimental Botany*, **62**, 3489-3499.

Yin X., Van Oijen M. & Schapendonk A. (2004) Extension of a biochemical model for the generalized stoichiometry of electron transport limited C3 photosynthesis. *Plant, Cell & Environment*, **27**, 1211-1222.

Yin X.Y. & Struik P.C. (2009b) Theoretical reconsiderations when estimating the mesophyll conductance to CO2 diffusion in leaves of C3 plants by analysis of combined gas exchange and chlorophyll fluorescence measurements. *Plant Cell and Environment*, **32**, 1513-1524.

Yin X.Y., Sun Z.P., Struik P.C., Van der Putten P.E.L., Van Ieperen W. & Harbinson J. (2011b) Using a biochemical C4 photosynthesis model and combined gas exchange and chlorophyll fluorescence measurements to estimate bundle-sheath conductance of maize leaves differing in age and nitrogen content. *Plant Cell and Environment*, **34**, 2183-2199.

Yongjian W., Yiwei J., Guosheng W., Feng Z & Lirong Z. (1998) Relationship between Photosynthetic Light Compensation Point and Tolerance to Low Temperature and Low Irradiance in Cucumber [J]. *Acta Horticulturae Sinica*, **2**.

Zhu X.-G., Long S.P. & Ort D.R. (2010) Improving photosynthetic efficiency for greater yield. *Annual Review of Plant Biology*, **61**, 235-261.

Figures.

Figure 1. Example of primary data obtained on tobacco plants. Panel **A**: light-response curves. Symbols show the response of A to decreasing $PPFD$ measured under ambient O_2 (closed circles) or 2% O_2 (open circles). Lines show the response of $Y(II)$ under ambient O_2 (solid line) or 2% O_2 (dotted line). Mean ± SE. Panel **B**: A/C_i response curves. Symbols show mean A ± SE plotted against mean C_i ± SE measured under ambient O_2 (closed circles) or 2% O_2 (open circles). Lines show mean $Y(II)$ ± SE for the same datapoints. $n=4$.

Tables.

Table 1. Acronyms, definitions, variables, and units used.

Symbol	Definition	Values / Units / References
A, A_{LOW}	Measured net assimilation, unspecified or under low O_2 respectively	µmol m^{-2} s^{-1}
A_{MOD}, A_{AMB}, A_J, A_C	Net assimilation under ambient O_2 modelled through Eqn 4, 16, 19, and 20 respectively	µmol m^{-2} s^{-1}
A_{SAT}	CO_2 saturated A, under the *PPFD* of the *A/C$_C$* curves	µmol m^{-2} s^{-1}
b	y-intercept of the linear fit of *Y(II)* against *Y(CO$_2$)*, it represent the fraction of *Y(II)* not used for RPP + PCO cycles, i.e. the fraction of *Y(II)* used by alternative electron sinks	dimensionless (Valentini *et al.*, 1995)
C_a	CO_2 concentration in the cuvette as measured by the IRGA	µmol mol^{-1}
C_C	CO_2 concentration at the site of Rubisco carboxylation $C_C = C_i - \frac{A}{g_M}$	µmol mol^{-1}
CCM	Carbon Concentrating Mechanism	
CE_{AMB}, CE_{LOW}	Initial slope of the *A/C$_C$* curve under ambient O_2, or low O_2 respectively	mol m^{-2} s^{-1}
C_i^*	C_i–GA compensation point, i.e. C_i in which GA=0 $C_i^* = \Gamma^* - \frac{R_{LIGHT}}{g_M}$	µmol mol^{-1} [Eqn 2.41 in (von Caemmerer, 2000)]
C_i, C_{iAMB}, C_{iLOW}	CO_2 concentration in the substomatal cavity as calculated by the IRGA, unspecified, under ambient or low O_2 respectively	µmol mol^{-1} (Eqn 1-18 in the Li-COR 6400 manual)
C_{i50}	C_i which half-saturates A	
EFT	Excel based Fitting Tool	
F	Photorespiration rate, or rate of photorespiratory CO_2 evolution $F = 0.5 \cdot V_O$	µmol m^{-2} s^{-1}
F	Chlorophyll *a* fluorescence signal (corresponding to fluorescence yield because normalized to measuring light)	µmol m^{-2} s^{-1}
F_V/F_M	*Y(II)* measured on dark adapted leaves	dimensionless
GA	Gross assimilation $GA = A + R_{LIGHT}$. GA represents the net biochemical CO_2 uptake $GA=V_C-F$	µmol m^{-2} s^{-1}
GA_{MOD}	Gross assimilation under ambient or low O_2 modelled through Eqn 3	µmol m^{-2} s^{-1}
GA_{SAT}	Light-saturated GA, under the CO_2 concentration of light-curves	µmol m^{-2} s^{-1}
g_M	Mesophyll conductance to CO_2	mol m^{-2} s^{-1}
IRGA	Infra-Red Gas Analyser	
J	Electron transport rate delivered to NADP$^+$ and used by the RPP and PCO cycles	µmol m^{-2} s^{-1}
J_{SAT}	Light-saturated Electron transport rate under the CO_2 concentration of light-curves, J_{MAX} in the notation of Farquhar	µmol m^{-2} s^{-1}
k	Slope of the linear fit of *Y(II)* against *Y(CO$_2$)*	dimensionless (Valentini *et al.*, 1995)
K_C	Rubisco Michaelis-Menten constant for CO_2	µmol mol^{-1}
$K_C(1+O/K_O)$	Rubisco Michaelis-Menten constant for CO_2 in the presence of O_2 competitive inhibition, without respiratory and photorespiratory CO_2 release	µmol mol^{-1}
K_O	Rubisco Michaelis-Menten constant for O_2	µbar
LCP	PPFD–A compensation point, i.e. *PPFD* when A=0. At the LCP the rate of Rubisco carboxylation equals the rate of respiration + photorespiratory CO_2 release ($V_C=R_{LIGHT}+F$). In non-photorespiratory conditions, when $V_C=R_{LIGHT}$, the LCP is lower.	µmol m^{-2} s^{-1}
L_S	Stomatal limitation to photosynthesis	dimensionless
m	Curvature of the non-rectangular hyperbola fitted to describe the *PPFD* dependence of *GA*	dimensionless
O, O_{AMB}, O_{LOW}	O_2 concentration in mesophyll cells (in air at equilibrium): unspecified, under ambient or low O_2 respectively	O_H 210000 µmol mol^{-1} O_L 20000 µmol mol^{-1}
PCO	Photosynthetic Carbon Oxygenation (cycle)	
PGA	3-phosphoglyceric acid	
PPFD	Photosynthetic Photon Flux Density	µmol m^{-2} s^{-1}
$PPFD_{50}$	*PPFD* which half saturates either *GA* or *J*	µmol m^{-2} s^{-1}
PSII	Photosystem II	
Q_A	Primary quinone acceptor of PSII	
R_{DARK}	Dark respiration	R_{DARK} >0 µmol m^{-2} s^{-1}
R_{LIGHT}	Respiration in the light; also known as respiration in the day	R_{LIGHT} >0 µmol m^{-2} s^{-1}
RPP	Reductive pentose phosphate (cycle); also known as Calvin-Benson-Bassham cycle or photosynthetic carbon reduction cycle	
Rubisco	Ribulose bisphosphate carboxylase oxygenase	
RuBP	Ribulose-1,5-bisphosphate	
s	Fraction of *PPFD* harvested by PSII obtained by curve fitting according to Yin, it depends on leaf absorptance, PSII optical cross section, and accounts for engagement of alternative electron sinks and cyclic electron flow	dimensionless (Yin *et al.*, 2004)
$S_{C/O}$	Rubisco specificity factor $S_{C/O} = \frac{V_{OMAX}K_C}{V_{CMAX}K_O}$	dimensionless
TPU	Triose Phosphate Utilisation	
V_C	Rubisco carboxylation rate	µmol m^{-2} s^{-1}
V_{CMAX}	CO_2-saturated Rubisco carboxylation rate	µmol m^{-2} s^{-1}
V_O	Rubisco oxygenation rate	µmol m^{-2} s^{-1}
V_{OMAX}	O_2-saturated Rubisco oxygenation rate	µmol m^{-2} s^{-1}
Y(CO$_2$)	Quantum yield for CO_2 fixation $Y(CO_2) = \frac{GA}{PPFD}$; also known as Φ_{CO2}	dimensionless
Y(CO$_2$)$_{LL}$	Initial (or maximum) quantum yield for CO_2 fixation; Φ_{CO2LL} in the notation of Yin	dimensionless
Y(II), *Y(II)$_{AMB}$*, *Y(II)$_{LOW}$*	Yield of photosystem II $Y(II) = \frac{F'_M - F_S}{F'_M}$; also known as Φ_2 or Φ_{PS2}, unspecified, under ambient or low O_2 respectively	dimensionless (Genty *et al.*, 1989)
Y(II)$_{LL}$	Initial *Y(II)* extrapolated to *PPFD*=0	dimensionless
Y(J)$_{LL}$	Initial (or maximum) quantum yield for electron transport, i.e. conversion efficiency of *PPFD* into *J*, K_{2LL} in the notation of Yin	dimensionless
αβ	Fraction of *PPFD* harvested by PSII according to Valentini, it lumps leaf absorptance and PSII optical cross section $\alpha\beta = \frac{4}{k}$	dimensionless (Valentini *et al.*, 1995)
Γ	C_i–A compensation point, i.e. C_i at which A=0 and $V_C=R_{LIGHT}+F$	µmol mol^{-1}
Γ^*	C_C–GA compensation point, i.e. C_C at which GA=0 and $V_C=F$ $\Gamma^* = 0.5 \frac{O}{S_{C/O}}$	µmol mol^{-1}
θ	Curvature of the non-rectangular hyperbola describing the *PPFD* dependence of *J*	dimensionless
ω	Curvature of the non-rectangular hyperbola describing the C_C dependence of *A*	dimensionless

Table 2. Minimum data required to obtain a desired output

Desired output	Minimum data necessary	Notes
s	Low O_2 fluorescence-light-response curve	
$\alpha\beta$	R_{LIGHT}, low O_2 fluorescence-A/C_i response curve or low O_2 fluorescence-light-response curve	In the EFT if both curves are available they can be pooled
$Y(CO_2)_{LL}$, LCP, GA_{SAT}, $PPFD_{50}$ (GA)	Light-response curve, R_{LIGHT}	If R_{LIGHT} is not available it can be derived in the same fitting
J_{SAT}, $PPFD_{50}$ (J)	Fluorescence-light-response curve, s or $\alpha\beta$	
$Y(II)_{LL}$	Fluorescence-light-response curve	
$Y(J)_{LL}$	$Y(II)_{LL}$, s or $\alpha\beta$	
$K_C(1+O/K_O)$ and V_{CMAX}	A/C_i response curve, R_{LIGHT}, g_M, Γ	If Γ is not available it can be derived in the same fitting. Ambient and low O_2 A/C_i curves if available can be fitted concurrently
Γ, CE, A_{SAT}, C_{i50}, L_S	A/C_i response curve under ambient or low O_2	
C_i^*	A/C_i response curve, R_{LIGHT}	
LCP	Light-response curve	R_{LIGHT} is preferably required if LCP is derived non-linearly (together with GA_{SAT})
g_M	Fluorescence-A/C_i response curve, $S_{C/O}$, R_{LIGHT}, s or $\alpha\beta$	
R_{LIGHT}	Fluorescence-light-response curve	
V_C, V_O, F	A and $Y(II)$ for each desired datapoint, R_{LIGHT}, s or $\alpha\beta$	
$S_{C/O}$, Γ^*	Low O_2 A/C_i response curve, A/C_i response curve, R_{LIGHT}	

Table 3. Output obtained by analysing the primary responses of tobacco plants reported in Figure 1. R^2 was >0.99, $n=4$. [†]additional output, [‡]methodological variants, n.f. no fit.

Logical Step	Output	Method	Ambient O_2 Mean	C.V. / %	EFT Location sheet, cell	Low O_2 Mean	C.V. / %	EFT Location sheet, cell
-	F_{DARK}	Measured	1.94	7	-	2.05	11	-
2	F_{LIGHT}	Fluorescence-Light (Yin)	1.75	17	2-3, N6	2.05	11	2-3, P6
2	F_{LIGHT}	Fitted (ambient O_2=low O_2)	1.96	10	2-3, Z12[†]	1.96	10	2-3, Z12[†]
2	F_{LIGHT}	Brooks-Farquhar	1.20	11	11, V14[†]	0.897	29	11, X14[†]
3	$Y(II)_{LL}$	Linear	0.723	2	2-3, N7 (AR11)	0.721	2	2-3, P7 (AT11)
3	$Y(II)_{LL}$	Quadratic	0.729	2	2-3, AR12[†]	0.738	2	2-3, AT12[†]
3	$Y(II)_{LL}$	Exponential	0.724	2	2-3, AR13[†]	0.723	2	2-3, AT13[†]
4	LCP	Hyperbola	31.8	14	4a, G5	27.5	12	4b, G5
4	LCP	Linear	30.8	14	2-3, AD48[†]	25.8	11	2-3, AF48[†]
4	GA_{SAT}	Hyperbola	26.0	13	4a, M3	39.9	7	4b, M3
4	$Y(CO_2)_{LL}$	Hyperbola	0.0562	7	4a, M2	0.0760	5	4b, M2
4	$Y(CO_2)_{LL}$	Linear	0.0576	9	6a-7, Q22[‡]	0.0791	5	6a-7, S22[‡]
4	$PPFD_{50}$	Hyperbola	296	12	4a, G6	339	4	4b, G6
4	m	Hyperbola	0.726	8	4a, M4	0.706	1	4b, M4
5	Φ	Hyperbola	0.123	15	5a M2	0.186	12	5b M2
5	Φ	Linear	0.120	7	11 X26[‡]	0.186	14	11 X33[‡]
5	A_{SAT}	Hyperbola	37.1	7	5a M3	34.3	7	5b M3
5	ω	Hyperbola	0.913	3	5a M4	0.971	1	5b M4
5	Γ	Hyperbola	56.3	1	5a M5	8.96	44	5b M5
5	Γ	Linear	56.4	1	11 W40[†]	9.23	17	11 Y40[†]
5	Γ^*	Hyperbola	42.0	4	5a G7	-2.10	237	5b G7
5	C_{50}	Hyperbola	222	7	5a G3	104	5	5b G3
5	L_S	Hyperbola	0.274	20	5a Z17[†]	0.104	26	5b Z17[†]
5	TPU	Horizontal maximum	12.5	7	5a Z25[†]	12.2	8	5b Z25[†]
6	s	Yin	-	-	-	0.439	3	6a-7, J6
6	k	*Valentini*	-	-	-	8.51	4	6b-7, G5
6	b	*Valentini*	-	-	-	0.0514	20	6b-7, G6
6	$\alpha\beta$	*Valentini*	-	-	-	0.471	4	6b-7, G7
7	$Y(J)_{LL}$	Yin	0.317	5	6a-7, J8[‡]	0.316	5	6a-7, L8[‡]
7	$Y(J)_{LL}$	*Valentini*	0.317	4	6b-7, G8[‡]	0.316	4	6b-7, G9[‡]
9	J_{SAT}	*Valentini*	241	18	8-9, M2[‡]	-	-	-
9	θ	*Valentini*	0.673	11	8-9, M3[‡]	-	-	-
9	$PPFD_{50}$	*Valentini*	508	21	8-9, H6[‡]	-	-	-
9	J_{SAT}	*Yin*	289	19	8-9, M2[‡]	-	-	-
9	θ	*Yin*	0.600	14	8-9, M3[‡]	-	-	-
9	$PPFD_{50}$	*Yin*	641	23	8-9, H6[‡]	-	-	-
9	J_{SAT}	*Bellasio*	223	16	8-9, M2[‡]	-	-	-
9	θ	*Bellasio*	0.523	22	8-9, M3[‡]	-	-	-
9	$PPFD_{50}$	*Bellasio*	524	22	8-9, H6[‡]	-	-	-
11	$S_{C/O}$	Φ from Hyperbola	2290	10	11, N6	-	-	-
11	$S_{C/O}$	Φ from Linear (Yin)	2404	4	11, N6[†‡]	-	-	-
11	$S_{C/O}$	From Γ^*, variant of Laisk	2501	4	5, Z9[†]			
12	g_M	J from Valentini	0.239	21	12, G6[‡]	-	-	-
12	g_M	J from Yin	0.154	18	12, Q6[‡]	-	-	-
12	g_M	J from Bellasio	0.307	20	12, Q6[‡]	-	-	-
13	V_{CMAX}	g_M from J Valentini	92.8	24	13a, M4[‡]	54	18	13b, M4[‡]
13	$K_C(1+C/K_O)$	g_M from J Valentini	278	35	13a, M5[‡]	45	47	13b, M5[‡]
13	V_{CMAX}	g_M from J Yin	n.f.	-	13a, M4[‡]	n.f.	-	13b, M4[‡]
13	$K_C(1+C/K_O)$	g_M from J Yin	n.f.	-	13a, M5[‡]	n.f.	-	13b, M5[‡]
13	V_{CMAX}	g_M from J Bellasio	114	38	13a, M4[‡]	90	49	13b, M4[‡]
13	$K_C(1+C/K_O)$	g_M from J Bellasio	476	50	13a, M5[‡]	152	59	13b, M5[‡]
13	V_{CMAX}	$V_{CMAXAMB}=V_{CMAXLOW}$, g_M from J Bellasio, K_C and K_O from Ethier	144	9	13b, AI15[†]	144	9	13b, AI15[†]